IVYSPRING INTERNATIONAL PUBLISHER

Theranostics

2023; 13(8): 2632-2656. doi: 10.7150/thno.82323

Review

Ratiometric optical probes for biosensing

Xiao Yang*, Congcong Li*, Peifeng Li✉, Qinrui Fu✉

Institute for Translational Medicine, The Affiliated Hospital of Qingdao University, College of Medicine, Qingdao University, Qingdao 266021, China.

* X. Yang and C. Li contributed equally to this work.

✉ Corresponding authors: E-mail: peifli@hotmail.com; fuqinrui2018@163.com.

Received: 2023.01.03; Accepted: 2023.04.15; Published: 2023.04.29

Abstract

Biosensing by optical probes is bringing about a revolution in our understanding of physiological and pathological states. Conventional optical probes for biosensing are prone to inaccurate detection results due to various analyte-independent factors that can lead to fluctuations in the absolute signal intensity. Ratiometric optical probes provide built-in self-calibration signal correction for more sensitive and reliable detection. Probes specifically developed for ratiometric optical detection have been shown to significantly improve the sensitivity and accuracy of biosensing. In this review, we focus on the advancements and sensing mechanism of ratiometric optical probes including photoacoustic (PA) probes, fluorescence (FL) probes, bioluminescence (BL) probes, chemiluminescence (CL) probes and afterglow probes. The versatile design strategies of these ratiometric optical probes are discussed along with a broad range of applications for biosensing such as sensing of pH, enzymes, reactive oxygen species (ROS), reactive nitrogen species (RNS), glutathione (GSH), metal ions, gas molecules and hypoxia factors, as well as the fluorescence resonance energy transfer (FRET)-based ratiometric probes for immunoassay biosensing. Finally, challenges and perspectives are discussed.

Keywords: optical probes, ratiometric probes, biosensing, self-calibration, analytes

Introduction

Sensing based on disease-associated analytes is an effective method for early diagnosis and subsequent treatment decision [1]. Biosensing has been one of the hot research topics in disease diagnostics, detection, and other biomedical fields, as a technique that generates signals associated with specific biomolecules of a disease and enables disease diagnosis by identifying the presence or change in concentration of disease-related analytes [2, 3]. Highly sensitive biosensing of clinically relevant analyte concentration changes is essential to ensure accurate disease diagnosis and reliable health monitoring [4, 5]. With the development of materials science and imaging technology, optical modalities such as fluorescence (FL) probes and chemiluminescence (CL) probes have been successfully integrated into biosensing [6-8]. Biosensing based on optical probes is bringing about a revolution in our understanding of physiological and pathological states.

In the last decade, optical probes have received widespread attention due to their advantages such as high sensitivity, high spatial and temporal resolution, and their wide range of applications in qualitative and quantitative sensing of disease-related analytes [9-12]. Optical probes can be divided into photoacoustic (PA) probes [13], photoluminescent (FL) probes [14], and self-luminescent probes [15] including bioluminescence (BL) probes, CL probes and afterglow probes, according to different imaging modalities. Optical probes with a single sensing signal may cause inaccurate assay results, which are susceptible to target-independent factors such as excitation source fluctuations, the specific microenvironment surrounding the probes, and variations in the local concentration of the probes [16, 17]. Ratiometric optical probes have become an important tool for biosensing due to their excellent built-in self-calibration signal correction capability to overcome the

limitations of optical probes with a single sensing signal [18, 19]. Ratiometric optical probes are based on analyte content changes in signal intensity caused by the acquisition of targets in two or more emission/absorption bands at different wavelengths, thus the influence of various external factors on the sensing results is avoided and the sensing accuracy is significantly improved [20-23]. Considering the many advantages of ratiometric optical probes, they can be used as a promising tool for fundamental applications and clinical research in biomedical fields.

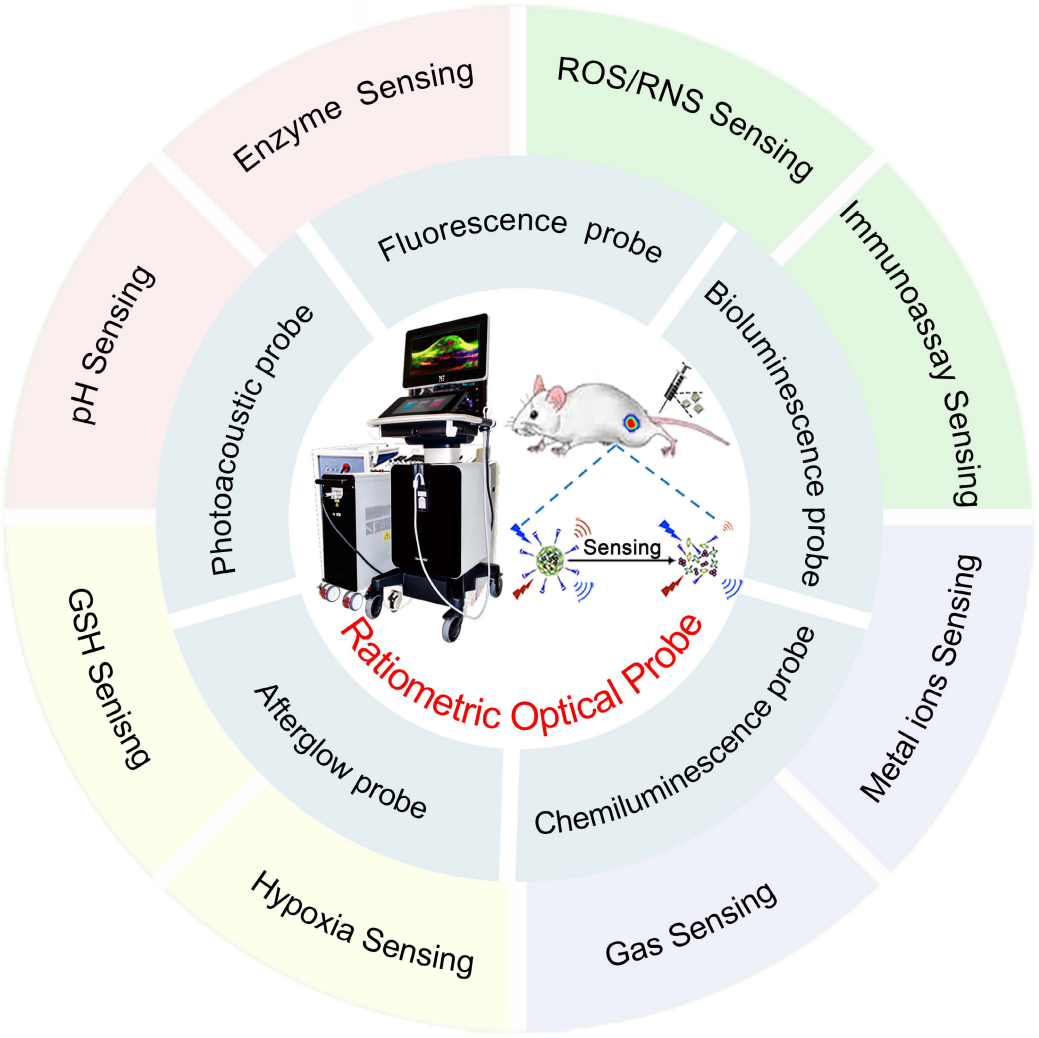

Figure 1. Schematic illustration of ratiometric optical probes (PA probes, FL probes, BL probes, CL probes and afterglow probes) for biosensing such as sensing of pH, enzymes, ROS, RNS, GSH, metal ions, gas molecules, hypoxia factors and immunoassay.

Table 1. Summary of the merits and drawbacks of different optical modalities

Classification	Merits	Drawbacks	Ref.
PA imaging	Deep tissue penetration; high imaging resolution, low scattering and dissipation in biological tissue	Low signal-to-noise ratio; diminished image contrast due to strong optical attenuation; a lower-bound on spatial resolution in deep tissue	[24-26]
FL imaging	Excellent sensitivity and selectivity; high spatiotemporal resolution; real-time detection; non-invasiveness; and low cost	Limited tissue penetration depth; severe interference from tissue absorption, scattering, and spontaneous fluorescence	[27-29]
BL imaging	No autofluorescence and phototoxicity; without external light excitation	Bioluminescence signal is relatively low and bioluminescence imaging rely on enzyme-initiated redox reactions to trigger luminescence	[30-32]
CL imaging	Effectively avoids light scattering; high sensitivity and signal-to-noise ratio, without external light excitation, no phototoxicity	Chemiluminescence signal is relatively weak and chemiluminescence signals are easily perturbed by internal stimuli such as redox microenvironment	[33-36]
Afterglow luminescence imaging	Effectively eliminated autofluorescence; no particular chemical mediator or exogenous enzyme	Luminescence decays with time, poor quantitative ability	[37-39]

Although there have been numerous reports on ratiometric probes in the recent years, most of which focus on specific types of probes or specific applications, to the best of our knowledge, few reviews have comprehensively summarized ratiometric optical probes for biosensing. Herein, we focus on the design principles of recently reported ratiometric optical probes and their applications in biosensing. The advancements and sensing mechanism of optical probes (Table 1) including PA probes, FL probes, BL probes, CL probes and afterglow probes are first discussed. The versatile design strategies of these ratiometric optical probes are discussed along with a broad range of applications for biosensing such as sensing of pH, enzymes, reactive oxygen species (ROS), reactive nitrogen species (RNS), glutathione (GSH), metal ions, gas molecules, hypoxia factors and immunoassay (Figure 1). Finally, challenges and perspectives are discussed.

Classification of ratiometric optical probe

Ratiometric molecular probes and ratiometric nanoprobes are collectively referred to as ratiometric probes. Molecular probes are systems that form strong and inherently irreversible bonds with their target analyte [40]; Nanoprobes are constructed primarily by functionalizing nanomaterials with specific molecular ligands [41, 42]; Alternatively, some nanoprobes can be obtained by combining molecular probes with nanoparticles [43, 44]. Therefore, in the following sections, the molecular probes and the nanoprobes are represented as probes. Ratiometric optical probes are classified according to different mechanisms as ratiometric PA probes, ratiometric FL probes, and ratiometric self-luminescent probes including ratiometric BL probes, ratiometric CL probes and ratiometric afterglow probes.

Ratiometric PA probes

PA probe is a non-invasive biomedical diagnostic tool that utilizes the PA effect to convert absorbed photons into sound waves [45, 46]. The PA probe combines the advantages of optical and ultrasound with the features of strong contrast and high spatial resolution to provide a favorable strategy for the study of physiological and pathological states of organisms [47-50]. Ratiometric PA probe is based on self-calibration of the signal intensity and recording of the signal fluctuations induced by the analytes [51]. There are two design strategies for the ratiometric PA probe: one strategy is that a single probe with an analyte-insensitive reference signal and an analyte-responsive sensing signal to achieve the ratio measurement [52]; another strategy is that the probe achieves the ratio measurement by reversible signal changes in the responses of an analyte [53]. The built-in self-calibration of ratiometric PA probes enables more sensitive and reliable detection, providing an essential means to study the morphological structure, metabolic function, physiological and pathological properties of biological tissues (**Figure 2**) [54-56].

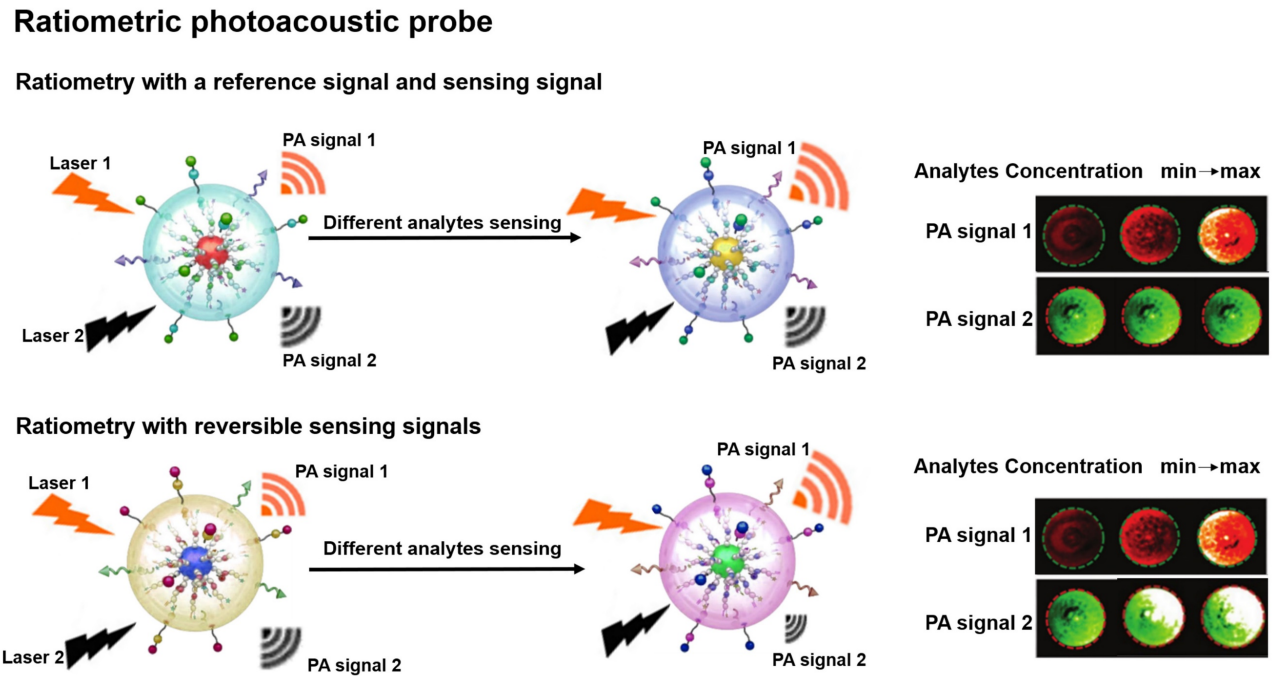

Figure 2. Schematic illustration of ratiometric PA probes for sensing *in vitro* and *in vivo* and the PA signal changes with the concentration of analytes. Adapted with permission from [68], Copyright 2019 American Chemical Society.

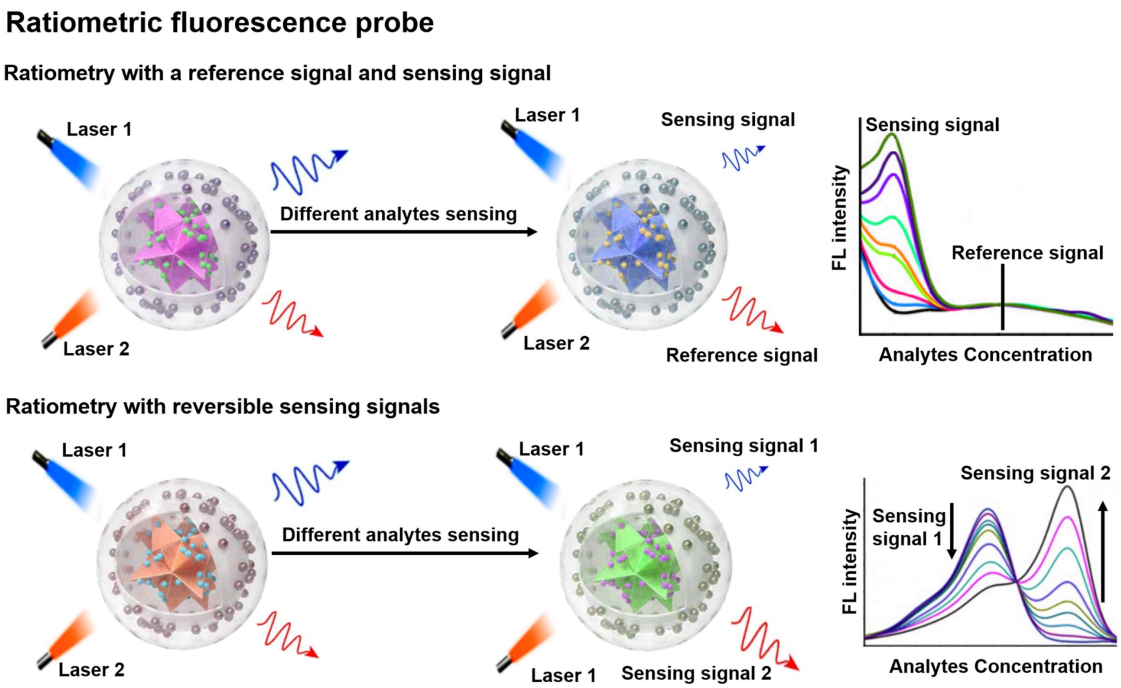

Figure 3. Schematic representation of the sensing principle of ratiometric FL probes and the FL intensity varies with the analyte concentration. Adapted with permission from [69], Copyright 2022 Wiley-VCH.

Ratiometric FL probe

FL is a photoluminescent phenomenon that relies on the emission of excited singlet relaxed photons [57, 58]. Compared to non-optical probes, FL probes offer superior sensitivity and strong spatial resolution, enabling non-invasive and real-time sensing of biological tissues [59-62]. Traditional FL probes are susceptible to analytically independent factors that cause drastic changes in the intensity of the background signal, which in turn affect the FL signal results. Ratiometric FL probes can adequately overcome the above issues by combining the reference and sensing signals, or by incorporating both reversible signal variations in response to the analytes into a single probe (**Figure 3**) [18, 63, 64]. The proposed mechanism of ratiometric FL probes can effectively improve the sensing contrast and provide high detection sensitivity for disease diagnosis, and will have a large scope in biomedical applications [65-67].

Fluorescence resonance energy transfer (FRET)-based probes belong to the class of FL probes, which are small molecule probes designed based on the FRET effect and have been widely used for selective detection in living organisms [70]. The general principles for the design of FRET-based ratiometric probes are the proximity of the donor-acceptor pair and the overlap of the emission spectrum of the donor with the absorption spectrum of the acceptor, as well as the need for a reaction unit that can be used as a specific recognition group [71]. When a FRET probe is exposed to a disease-relevant target analyte, the FRET effect is initiated or blocked and, in turn, a change in the FL signal ratio can be observed, which ultimately determines whether the target analyte is present or not (**Figure 4**) [72]. FRET-based ratiometric probes thus provide a unique way to sense biologically and environmentally important analytes and can reveal the physiological and pathological function of these analytes.

Ratiometric self-luminescence probe

BL probes, CL probes and afterglow probes all belong to the category of self-luminescent probes, which can effectively eliminate external light interference and achieve high sensitivity sensing results [74]. BL refers to light emitted by catalytic reactions between bioluminescent enzymes (luciferase) and substrates (luciferin and other small molecules) [75-77]. In BL process, the energy generated by an enzymatically catalyzed chemical reaction excites electrons to excited state, and photons are emitted as light when the electrons return to their ground state [78]. CL can be described as the phenomenon of emission of photons when electrons return from the excited state to the ground state during a chemical reaction. Compared to photoluminescent probes, CL probes are a valuable sensing tool because they provide their own light source and thus attenuate autofluorescence and light scattering effects [79, 80]. Afterglow luminescence requires pre-illumination of

the afterglow agent. The excitation energy in defects is captured by the afterglow agents, and the stored energy is slowly released by photons during physical activation, thus eliminating autofluorescence [81, 82]. Ratiometric self-luminescent probes typically integrate analytically sensitive signals as sensing signals and analytically insensitive signals as reference signals into a single probe, or a single probe with analytically responsive reversible signal variations, which do not rely on real-time excitation of exogenous light to detect the luminescence signal, and can effectively eliminate the interference of self-luminescence and achieve high-sensitivity sensing (**Figure 5**) [38, 83].

Ratiometric optical probes for biosensing

Abnormal pH, ROS, RNS, GSH, enzymes, metal ions, gases, and hypoxia factors in the tumor microenvironment (TME) plays a major role in managing homeostasis processes [85-87]. Thus, the sensing of pathological factors in the TME provides new insights for the diagnosis or discovery of certain diseases. Recently, ratiometric optical probes have been frequently used for the sensing of endogenous pathological factors due to their advantage of being free from external environmental interference, leading to more reliable and accurate sensing results [88, 89].

pH sensing

Intracellular pH is closely related to cellular growth, differentiation and proliferation, and FRET-based ratiometric imaging using pH-sensitive probe provides a powerful tool to assess the pH of cancer cells [90]. For example, Yu and co-workers successfully prepared a FRET-based ratiometric bispyrene-fluorescein hybrid probe (PF), consisting of a pH-insensitive bispyrene unit as an energy donor and a pH-sensitive fluorescein as an energy acceptor, for sensing of pH changes in HeLa cells (**Figure 6A**) [91]. *In vitro* emission spectrum analysis demonstrated that the emission from fluorescein at 526 nm remarkably enhanced with increasing pH, whereas that from pyrene excimer at 459 nm was significantly reduced (**Figure 6B**). This is due to the change in the structure of the fluorescein cyclolactam in the PF probe from the ring closure to ring-opening with increasing pH, which turns on the FRET effect, resulting in a decrease in the blue emission intensity of the pyrene molecule as a donor and an increase in the green emission intensity of the fluorescein as an acceptor. As shown in **Figure 6C**, the corresponding FL signal ratio (I_{526}/I_{459}) thus increased from 0.26 to 5.82 as the pH increased from 3 to 10. In addition, the potential of the intracellular ratiometric FL signal for pH sensing was further evaluated. As shown in Figure 6D, as the pH increased from 4.0 to 8.0, the signal strength within the HeLa cell from the green channel increased significantly, whereas the that from the blue channel decreased significantly, resulting in a significant enhancement of the ratio from 0.27 to 2.25. These results demonstrated the potential of PF probes for quantitative sensing of pH changes in living cells with a wide range of applications in the biomedical field.

FRET-based ratiometric probes can not only sense pH changes at the cellular level, but can also be applied at the *in vivo* level to provide important information on the occurrence and development of diseases [92-94]. Among them, upconversion nanoparticles (UCNPs) with excellent capability of bioanalysis and bioluminescence have drawn

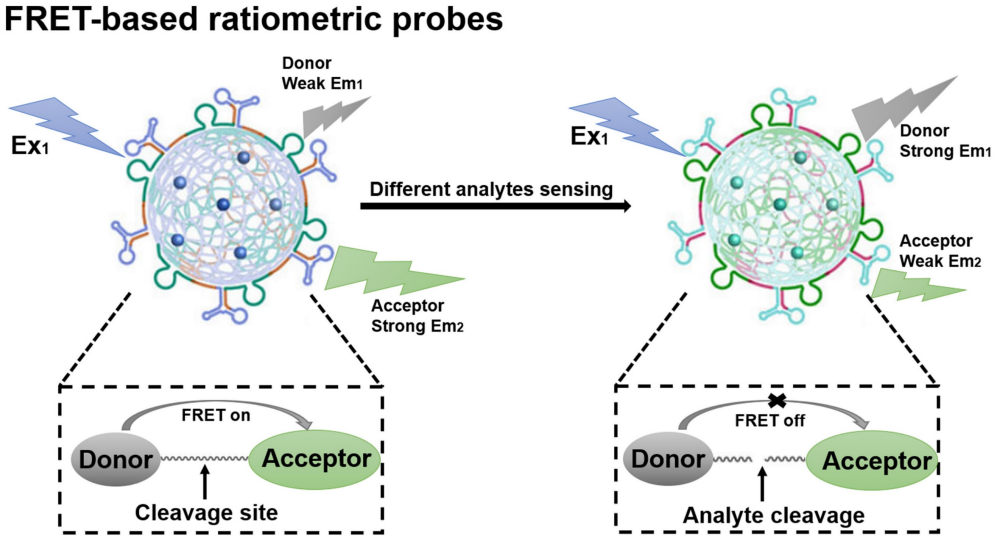

Figure 4. Schematic illustration of the sensing principle of FRET-based ratiometric probes. The cleavage of the covalent link between the donor and acceptor by the analyte causes the FRET system to shut down. Adapted with permission from [73], Copyright 2023 American Chemical Society.

increasing attention [95, 96]. For example, Xian and co-workers fabricated a FRET system (UCNPs@SiO_2-Ag_2S) consisting of GSH and mercaptopropionic acid (MPA) co-modified Ag_2S nanodots (GM-Ag_2S NDs) as energy acceptor and silica-encapsulated UCNPs as energy donor for real-time sensing of pH in tumor-bearing zebrafish (**Figure 6E**) [97]. Under excitation at 980 nm, the GM-Ag_2S NDs, as a sensing signal, showed an enhanced luminescence intensity at 795 nm with increasing pH; while the UCNPs, as a reference signal, showed a constant signal at 540 nm (**Figure 6F**). As a result, its luminescence signal ratio (I_{795}/I_{540}) increased as a function of pH (**Figure 6G**). After injecting the probes into zebrafish, the changes in pH *in vivo* were observed *via* ratiometric FL imaging. As shown in **Figure 6H, I**, the green signal at 540 nm remained almost unchanged, while the red signal at 795 nm increased with the increasing pH, resulting in a pH-dependent enhanced I_{795}/I_{540} ratio. The results demonstrated that FRET-based ratiometric probes can be used for real-time *in vivo* pH sensing and significantly advance the application of ratiometric optical probes in biomedicine.

Energy acceptors and donors for FRET-based probes can be provided not only by fluorescent molecules or nanoparticles, but also by fluorescent proteins [98]. Fluorescent proteins are extremely well suited for use as optical sensors in living cells due to their unique optical signaling mechanism and their vulnerability to the surrounding chemical environment and protein-protein interactions upon expression. For example, Malli *et al*. designed a ratiometric fluorescent protein FRET biosensor (pH-Lemon) consisting of a pH-insensitive cyan

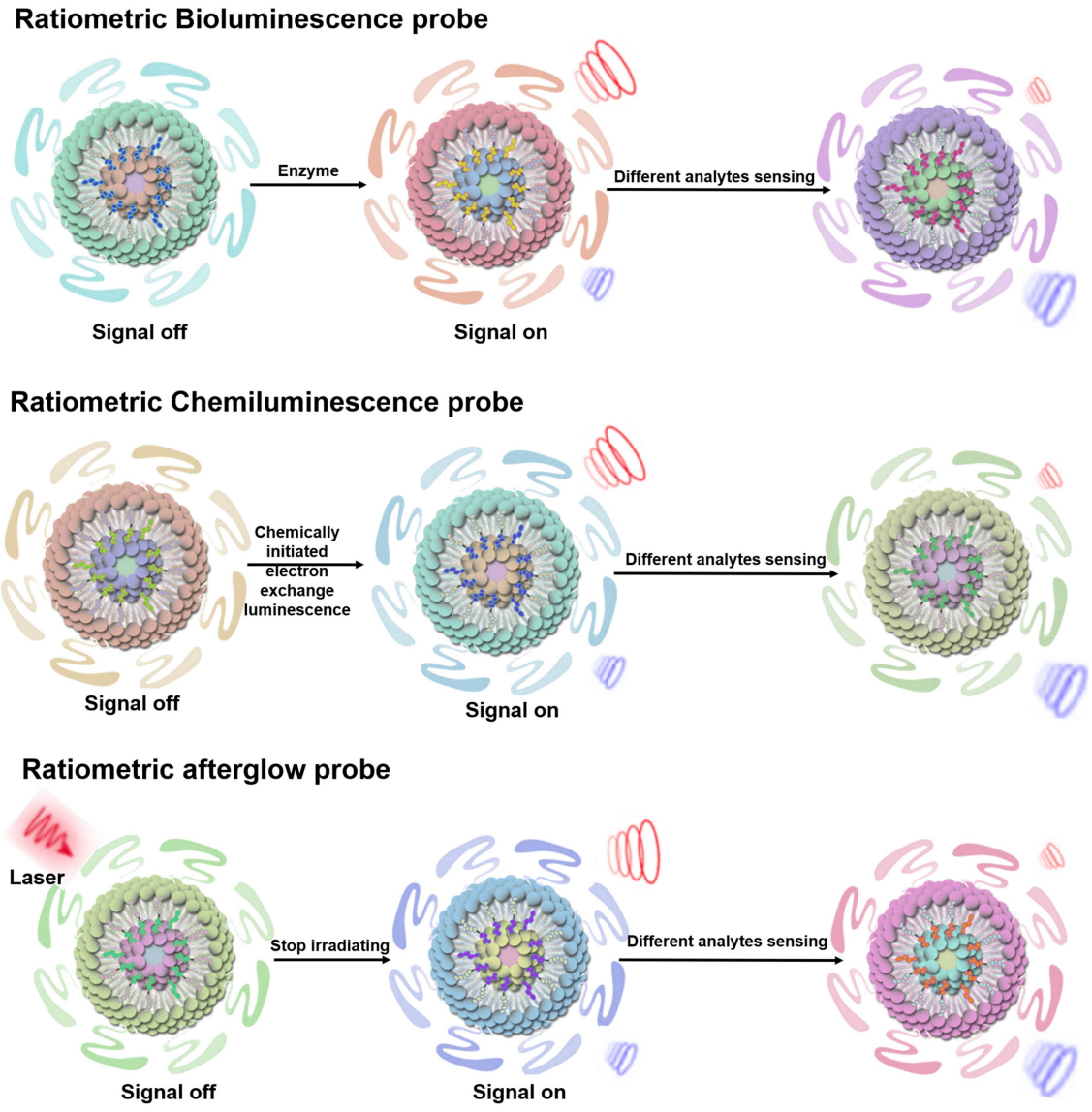

Figure 5. Schematic illustration of the sensing principle of ratiometric self-luminescence probes. Adapted with permission from [84], Copyright 2022 American Chemical Society.

fluorescent protein (CFP) variant (mTurquoise2) and a highly pH-sensitive enhanced yellow fluorescent protein (EYFP) for sensing the local pH dynamics of subcellular microstructures in living cells [99]. At neutral to alkaline pH values, the C-terminus of the mTurquoise2 (FRET donor) was fused to the N-terminal end of the EYFP (FRET acceptor) via a small, flexible linker, leading to yield high FRET effect. Under acidic conditions, the pH-sensitive EYFP underwent protonation, which significantly reduced yellow FL, while cyan FL increased due to FRET effect was quenched; the corresponding FL signal ratio (F_{EYFP}/F_{CFP}) thus decreased with decreasing pH values. These results indicated that fluorescent protein-based ratiometric FL probes could be used for sensing of pH changes.

In addition to ratiometric FL probes, ratiometric PA probes can also be used for pH sensing *in vivo*. For example, Pu *et al.* developed an activatable PA probes (SNOS) consisting of an inert PA-based semiconducting oligomer (SO), an amphiphilic triblock copolymer (PEG-b-PPG-b-PEG), and a pH indicator and enhancer (pH-BDP) for *in vivo* sensing of pH changes (**Figure 6J**) [100]. As shown in **Figure 6K**, the PA signal at 680 nm remained almost unchanged, while the signal at 750 nm decreased significantly with decreasing pH, due to the fact that the pH-BDP underwent an efficient protonation-deprotonation process with decreasing pH, hence resulting in an increase of the PA_{680nm}/PA_{750nm} ratio as a function of pH. As shown in **Figure 6L**, the PA signal ratio at pH = 5.4 was increased by a factor of 3.44 compared to that at pH = 7.4, while the PA signal ratio at pH = 5.5 was increased by 1.91-fold compared to that at pH = 6.4. Therefore, the PA_{680nm}/PA_{750nm} ratio can be used to efficiently sense pH in physiological and pathological conditions. After local injection of the probe into the muscles or into the Hela xenografts tumor of nude mice, the intensity of the PA signal at 750 nm in Hela xenografts tumor was significantly reduced compared to that in the muscle tissue (**Figure 6M**), resulting in the PA_{680nm}/PA_{750nm} ratio of tumor was 1.9-fold higher than that of muscle tissue (**Figure 6N**) due to tumor acidic microenvironment. In addition, the PA_{680nm}/PA_{750nm} ratio showed an excellent linear relationship with the pH value, thus enabling *in vivo* sensing of pH changes *via* ratiometric PA signals.

In addition to ratiometric photoluminescence (FL) probes and ratiometric PA probes, ratiometric self-luminescence probes can also be used for *in vivo* sensing of pH changes. For example, Lippert and colleagues developed a pH responsive ratiometric CL probe with a chemiluminescence resonance energy transfer (CRET) effect (named as ratio-pHCL-1) consisting of a pH-sensitive carbon fluorescein and a chemiluminescent scaffold (acrylamide 1,2-dioxetane) for pH sensing (**Figure 6O**) [101]. The CL intensity at 580 nm increased significantly, while that at 530 nm remained almost unchanged with increasing pH due to the CRET effect, leading to the CL signal ratio ($CL_{580\ nm}/CL_{530\ nm}$) increased as a function of pH (**Figure 6P**). After intravenous administration, the CL imaging at 580 nm (**Figure 6Q**) and 540 nm (**Figure 6R**) were performed by using an IVIS Spectrum. The corresponding ratiometric CL signals ($Flux_{580\ nm}/Flux_{540\ nm}$) in the peritoneal cavity of mice were quantitatively calculated (**Figure 6S**), the results showed that a positive correlation between ratiometric CL signals ($Flux_{580\ nm}/Flux_{540\ nm}$) and *in vivo* pH value. This result demonstrated the potential of the ratiometric self-luminescent probes to enjoy a wide range of intracellular and *in vivo* pH sensing applications.

Sensing of ROS

ROS are endogenously generated essential signaling-reactive molecules, such as hydrogen radicals ($^{\cdot}OH$), superoxide (O_2^{-}), hypochlorous acid (HOCl/HClO)/hypochlorite (^{-}OCl), singlet state oxygen ($^1O_2$), hydrogen peroxide (H_2O_2), *etc.*, which play important roles in regulating numerous events of physiological and pathological processes [102-109]. Therefore, the establishment of reliable *in vivo* ROS sensing methods in real-time is of great importance for the diagnosis and treatment of diseases. For example, Zhang and co-workers developed a ratiometric FL probe (ErBG@IR808) consisting of HClO responsive IR808 fluorophores modified Er nanoparticles (ErNPs) with a bioactive Glass (BG) scaffold for ROS sensing [110]. There was an absorption competition induced emission (ACIE) effect between IR808 and ErNPs, resulting in quenching of the emission at 1525 nm of ErBG scaffolds excited at 808 nm (F_{808ex}). In the presence of HClO, the quenched FL signal of ErBG was recovered under excitation at 808 nm (F_{808ex}) due to HClO triggered degradation of IR808, while the 1525 nm emission upon 980 nm excitation (F_{980ex}) remained unaffected. Therefore, there was a positive correlation between the FL intensity ratio (F_{808ex}/F_{980ex}) and the concentration of ClO^{-}. After intravenous injection of the probe into the inflammatory mice, F_{808ex} gradually increased with the time after injection and reached the maximum value at 7 h post-injection, while F_{980ex} remained constant, resulting in an increase in F_{808ex}/F_{980ex} as a function of time. The results illustrated the excellent capability of the ErBG@IR808 probe to sense HClO secreted by inflammatory cells *via* the ratiometric FL signal.

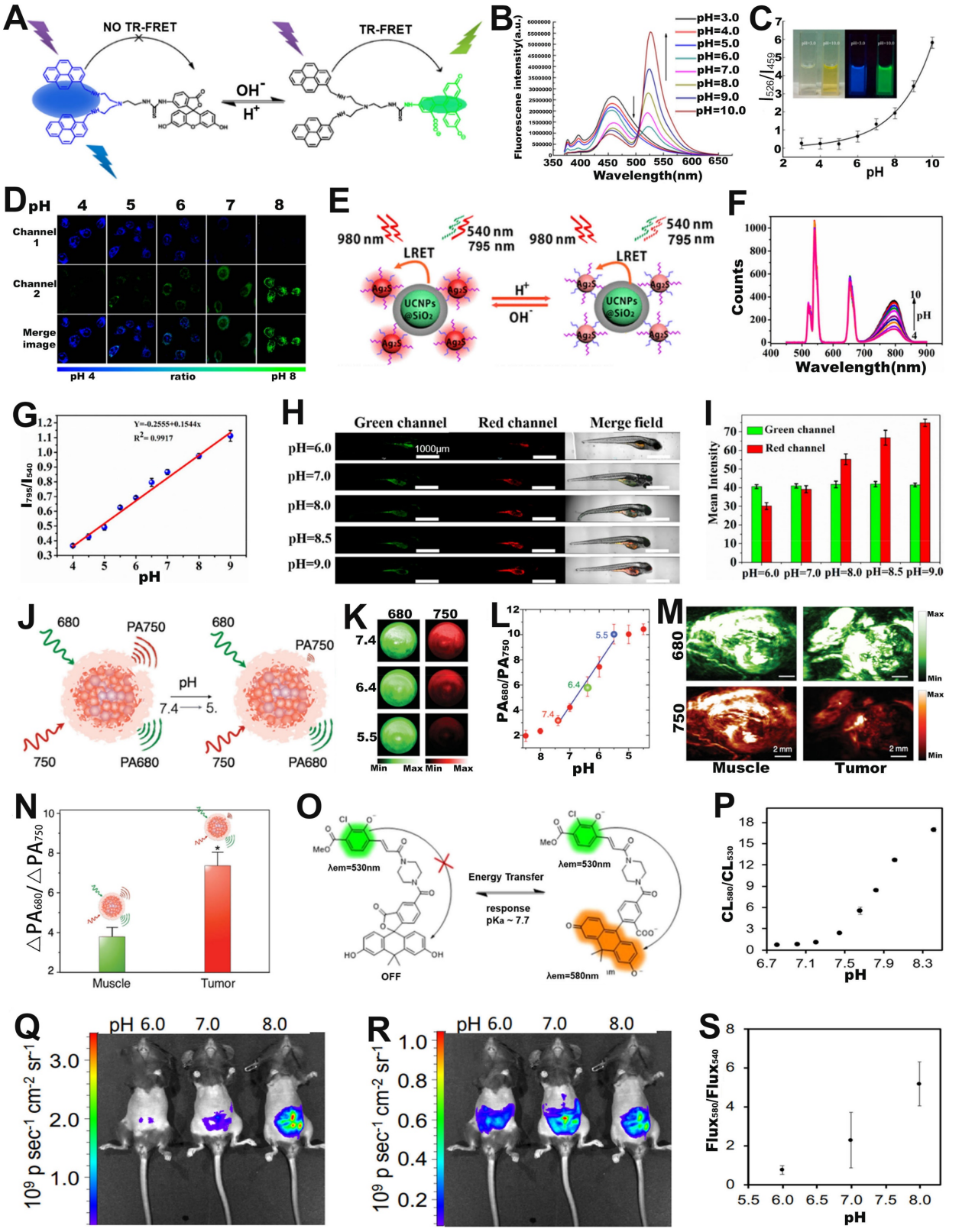

Figure 6. (**A**) The structure and response mechanisms of FRET-based ratiometric bispyrene-fluorescein hybrid probe. (**B**) The FL intensity changes of PF probe with pH value. (**C**) The relationship between pH and FL signal ratio (I_{526}/I_{459}). (**D**) Confocal FL image after incubation of probe with Hela cells. (**E**) Schematic diagram of pH sensing mechanism of UCNPs@SiO_2-Ag_2S probe. (**F**) The luminescence spectrum changes with pH value. (**G**) The FL signal ratio as a function of pH. (**H**) Confocal images of zebrafish with probes incubated at different pH, and (**I**) corresponding luminescence intensity ratio. (**J**) Proposed mechanism of ratiometric probe SNOS for pH sensing. (**K**) PA imaging at different pH values. (**L**) The relationship between pH value and PA signal ratio. (**M**) PA images of muscle and tumor site after injection of probe, and (**N**) corresponding $PA_{680\ nm}/PA_{750\ nm}$ ratio. (**O**) Chemical structure and sensing mechanism of ratiometric CL probe. (**P**) Relationship between pH and $CL_{580\ nm}/CL_{530\ nm}$. CL images of ratio-pHCl-1 injected into the mice using a (**Q**) 580 nm filter or (**R**) 540 nm filter in the IVIS Spectrum. (**S**) The relationship between pH value and $Flux_{580}/Flux_{540}$. (**A-D**) Adapted with permission from [91], Copyright 2014 American Chemical Society. (**E-I**) Adapted with permission from [97], Copyright 2019 American Chemical Society. (**J-N**) Adapted with permission from [100], Copyright 2016 WILEY-VCH. (**O-S**) Adapted with permission from [101], Copyright 2020 American Chemical Society.

FRET-based ratiometric probe can also be used for ROS sensing. For example, Zhao *et al.* developed a ratiometric FL probe (CARSH) consisting of a HOCl-insensitive coumarin-ethylene as FRET energy donor and a HOCl-sensitive rhodamine as FRET energy acceptor for the quantitative sensing of HOCl in living organisms (**Figure 7A**) [111]. In the probe, the coumarin-ethylene had an FL peak at 405-550 nm (blue light) and the rhodamine had an FL peak of at 550-650 nm (red light). Upon incubation with HOCl, the thiohydrazide moiety of rhodamine (acceptor) reacted with HOCl to open the thiohydrazide spiro ring, and then the energy of FRET energy donor (coumarin-ethylene) was transferred to the FRET energy acceptor (rhodamine) through the FRET effect, which eventually led to enhanced red-light emission and reduced blue light emission (**Figure 7B**). The FL signal ratio (I_{580}/I_{490}) increased with the increasing HClO concentration (**Figure 7C**), thus can be used for ROS sensing. RAW264.7 cells were incubated with CARSH probe and CARSH probe + lipopolysaccharide (LPS, which stimulated cells to produce HOCl), respectively, a significant increase in the FL signal ratio (red/blue) corresponding to the group with the addition of LPS was observed (**Figure 7D, E**). The results indicated that the FRET-based ratiometric CARSH probe can be used for sensing of HOCl at the cellular level.

Furthermore, ratiometric FL probe can also be used for sensing of HOCl at the *in vivo* level. Yang and co-workers fabricated a ratiometric FL probe (DCNP@SeTT) consisting of Er^{3+}-doped down-conversion nanoparticles (DCNP), polyethylene glycol phospholipids (DSPE-PEG), and a NIR-II FL dye (SeTT) for the effective sensing of ROS *in vivo* (**Figure 7F**) [112]. DCNP@SeTT had two specific FL peaks at 1150 nm and 1550 nm, respectively. After incubation of the probe with HClO, the FL signal of the SeTT at 1150 nm was weakened due to oxidation of the SeTT by HClO, while the FL signal of the DCNP at 1550 nm, which was used as the internal reference signal, showed negligible changes (**Figure 7G**). Therefore, there was a negative correlation between HClO concentration and FL signal ratio ($I_{1150\ nm}/I_{1550\ nm}$) (**Figure 7H**). After injecting the probe into the mice, the FL images at 1150 and 1550 nm were observed to explore the ability of the probe to sense endogenous HClO (**Figure 7I**). As shown in **Figure 7J**, the presence of overexpressed ROS in the TME resulted in a gradual decrease in the FL signal ratio ($I_{1150\ nm}/I_{1550\ nm}$) with increasing time. These results indicated that the ratiometric FL probe successfully achieved rapid response and high selectivity for HClO sensing under *in vivo* physiological conditions and was a potentially promising tool for diseases diagnosis.

Ratiometric PA probes can also be used for ROS sensing [113-115]. For example, Pu and colleagues developed a ratiometric PA probe (SOA@NIR775) consisting of a semiconducting oligomer amphiphile (SOA, with an absorption peak at 680 nm) with a ROS-oxidizable aromatic unit and a ROS-inert dye NIR775 with an absorption peak at 780 nm for *in vivo* ClO^- sensing (**Figure 7K**) [116]. In the presence of HClO, the ROS-sensitive semiconductor skeleton in SOA was degraded, and the π-π stacking between the semiconductor skeleton in SOA and NIR775 was collapsed. As a result, the PA signal at 680 nm gradually decreased with the increase of HClO concentration, yet the PA signal at 780 nm remained unchanged (**Figure 7L, M**). Therefore, the PA signal ratio (PA_{780}/PA_{680}) increased linearly with ClO^- concentration (**Figure 7N**). As shown in **Figure 7O**, after intravenous administration, the PA signal at 780 nm increased over times, reaching a maximum value at 6 h post-injection, while the signal at 680 nm increased slightly. Therefore, the ratio of PA signal ($\Delta PA_{780}/\Delta PA_{680}$) at 6 h post-injection was 1.47 times higher than that at 2 h post-injection (**Figure 7P**). The results demonstrated that the ratiometric PA probe was an excellent tool to sense ClO^- levels under pathological conditions *in vivo* and had promising applications in the process of disease diagnosis.

Sensing of RNS

RNS refers to the interaction of nitric oxide (NO) with compounds including ROS, resulting in a series of nitrogen dioxide radicals ($NO_2^{\bullet}$), peroxynitrite ($ONOO^-$), and nitrate (NO_3^-) [117-119]. Overproduction of RNS is closely related to the occurrence of various diseases [120-122], and therefore, there will be a great scope for designing probes with high sensitivity and selectivity for RNS sensing in the biomedical domain. Chang and co-workers synthesized a FRET based ratiometric FL probe (PNCy3Cy5) for $ONOO^-$ sensing in living cells (**Figure 8A**) [123]. The energy donor (Cy3) and energy acceptor (Cy5) of the PNCy3Cy5 probe was linked by an acetyl piperazinyl hexyl group, and the ratiometric sensing mechanism of PNCy3Cy5 probe was based on modulating FRET between donor and acceptor. Upon incubation with $ONOO^-$, Cy5 was selectively oxidized to oxindole derivative and then the FRET effect was quenched, resulting in an increase in the FL emission intensity of Cy3 at 560 nm and a decrease in FL intensity of Cy5 at 660 nm (**Figure 8B**). Therefore, the $ONOO^-$ concentration showed a good positive correlation with the FL signal ratio (F_{560}/F_{660}). In addition, PNCy3Cy5 can specifically sense exogenous $OONO^-$ in living cells through ratiometric FL

imaging. In an *in vitro* RAW264.7 macrophages experiment, the FL signal ratio (F_{560}/F_{660}) remarkably enhanced after cells treated with SIN-1 (an $OONO^-$ donor) (**Figure 8C**). As shown in **Figure 8D**, a linear relationship between the FL signal ratio (F_{560}/F_{660}) and the SIN-1 concentration was observed. In addition, the F_{560}/F_{660} ratio of untreated and SIN-1 + minocycline ($OONO^-$ scavenger) treated RAW264.7 macrophages was lower than that of SIN-1-treated RAW264.7 macrophages. These results demonstrated that PNCy3Cy5 probe could explore the physiological mechanisms of $ONOO^-$ and investigate its role in related diseases, indicating its potential for advance biomedical sensing *in vivo*.

The ratiometric FL probe for NO sensing was described by Song *et al*. The probe (DCNP@MPS@IRNO) was comprised of a NO-responsive small-molecule organic dye (IR-NO) as a sensing signal unit, NO insensitive DCNP as a reference signal unit and mesoporous silica (MPS) (**Figure 8E, F**) [124]. In the absence of NO, cyanine fluorophore in IR-NO was coupled with the electron donor o-phenylenediamine

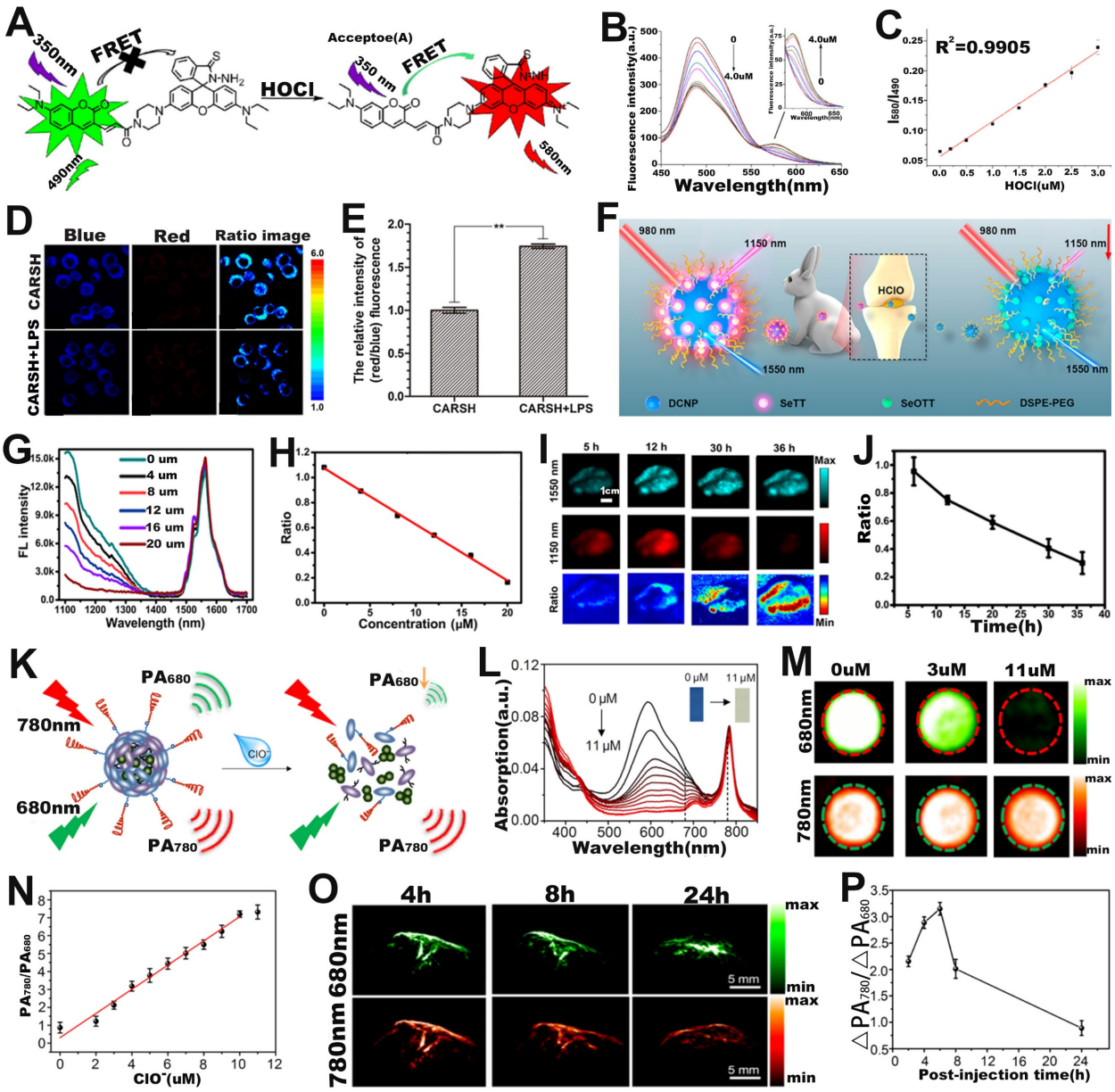

Figure 7. (**A**) Chemical structure and sensing mechanism of CARSH probe. (**B**) The FL intensity changes with the increase of HOCl concentration. (**C**) The relationship between HOCl concentration and FL signal ratio (I_{580}/I_{490}). (**D**) FL images of RAW264.7 cell after incubation with CARSH probe, and (**E**) corresponding ratio (red/blue) of FL intensity. (**F**) Proposed mechanisms of DCNP@SeTT@PEG probes for sensing of HClO within tumor and inflammation of rabbit models. (**G**) The FL intensity changes with the HClO concentration, and (**H**) corresponding $I_{1150\ nm}/I_{1550\ nm}$. (**I**) FL images in mice after intravenous injection of probe, and (**J**) $I_{1150\ nm}/I_{1550\ nm}$ as a function of time. (**K**) Mechanism of SOA@NIR775 probe for ratiometric PA sensing of ClO^-. (**L**) Changes in the absorption spectra of probes after the addition of different concentrations of ClO^-. (**M**) PA images of probes treated with different concentrations of ClO^-. (**N**) Variation of PA signal ratio with ClO^- concentration. (**O**) PA images of subcutaneous 4T1 tumor after intravenous injection of probes, and (**P**) corresponding PA signal ratio. (**A-E**) Adapted with permission from [111], Copyright 2016 Elsevier. (**F-J**) Adapted with permission from [112], Copyright 2020 American Chemical Society. (**K-P**) Adapted with permission from [116], Copyright 2017 American Chemical Society.

unit to generate photoinduced electron transfer (PET) effect, resulting in the quenching of FL of cyanine fluorophore. In the presence of NO, the o-phenylene-diamine unit in IR-NO can be converted into benzotriazole with weak electron donating capability, resulting in the blocking of the PET process and the restoration of the quenched FL, together with an emission wavelength of 1050 nm at 808 nm excitation. However, DCNP, as an internal reference signal, remained unaffected at 1550 nm upon excitation with a 980 nm laser. Therefore, the ratio signal (F_{808ex}/F_{980ex}) increased linearly with the increase of NO concentration (**Figure 8G**). Furthermore, *in vivo* liver injury ratiometric FL imaging experiments showed that the FL signal intensity at 1050 nm was enhanced; however, that at 1550 nm remained unchanged (Figure 8H). The FL signal of the probe at 1050 nm displayed a time-dependent increase within 90 min and reached the maximum value at 90 min post-injection. The FL signal ratio (F_{808ex}/F_{980ex}) thus increased with increasing time post-injection (Figure 8I). These results indicated that the DCNP@MPS@IR NO probe can effectively sense NO in the liver of APAP-induced liver injury mice and can be used for the visualization and early diagnosis of drug-induced liver injury.

Ratiometric afterglow probes are an emerging sensing platform, which can not only solve the problem of attenuation of afterglow intensity, but also eliminate the interference of external factors. Tang *et al.* developed a series of ratiometric afterglow probes (RAN) for NO and $ONOO^-$ sensing [125]. Among them, RAN-1, consisting of an afterglow substrate (MEHPPV), a NO-responsive molecule (NRM), a surfactant (F127) and an afterglow initiator (AI), can sense NO *in vivo* through the afterglow resonance energy transfer (ARET) strategy (**Figure 8J**). In the RAN-1 probe, MEHPPV, as an energy donor, can be triggered by AI producing $^1O_2$ to emit afterglow (AF1), and the AF1 energy was then transferred to the energy receptor (NRM) to release a longer wavelength afterglow (AF2) by the ARET effect. Upon treatment with NO, the weak electron acceptor (benzo[c][1,2,5] thiadiazole-5,6-diamine) of NRM reacted with NO to generate a stronger acceptor (5H[1,2,3]triazolo[4,5-f]-2,1,3-benzothiadiazole) of NRM-NO, which red-shifted its emission wavelengths due to enhanced effects of intramolecular charge transfer (ICT). As shown in **Figure 8K**, the FL intensity at 660 nm gradually increased and at 830 nm significantly increased with the increase of NO concentration, while the FL intensity of RAN-1 at 600 nm decreased. As shown in **Figure 8L**, after the incubated solutions were pre-irradiated by a 660 nm laser, a brighter AF2 at 830 nm and darker AF1 at 600 nm as a function of NO concentration was observed. Therefore, there was a good positive correlation between NO concentration and afterglow signal ratio (AF2/AF1) (**Figure 8M**). The RAN-2 was a $ONOO^-$ responsive probe (**Figure 8N**). Upon treatment with $ONOO^-$, as shown in **Figure 8O**, the FL intensity of the probe at 750-850 nm gradually decreased with the increase of $ONOO^-$ concentration. Furthermore, the signal at AF1 (820 nm) became darker, while at AF2 (600 nm) remained almost unchanged with the increase of $ONOO^-$ concentration (**Figure 8P**). Therefore, the AF2/AF1 signal ratio was linearly correlated with $ONOO^-$ concentration. After intravenous administration, the AF2/AF1 ratio in inflammation model mice was higher than that in healthy mice (**Figure 8Q, R**), suggesting that RAN-1 could sense NO levels in inflammation model. These results indicated that RAN-1 and RAN-2 were excellent ratiometric afterglow probes for sensing of NO and $ONOO^-$, respectively.

Sensing of enzyme

Enzymes participate in a wide range of important metabolic processes and are closely related to the activities of life [126-129]. Real-time sensing of enzymatic activity is of great significance for cancer diagnosis. Zhu and co-workers reported a *β*-gal enzyme activatable ratiometric near-infrared (NIR) FL probe (DCM-βgal) consisting of dicyanomethyl-4H-pyran (DCM) chromophore (NIR FL reporter) and *β*-gal cleavable unit (enzyme-active trigger) for sensing of *β*-gal enzyme (**Figure 9A**) [130]. DCM has the ability to regulate the electron donor of the phenolic group, and excellent donor-π-acceptor (D-π-A) characteristics. After DCM-βgal was incubated with *β*-gal enzyme, the C-O bond of DCM was hydrolyzed and released an electron-rich aglycon $DCM\text{-}O^-$, which enhanced ICT effect and significantly changed its emission wavelength. As shown in **Figure 9B**, with the increase of *β*-gal concentration, the FL signal of the probe at 500 nm was weakened and a new peak appeared at 685 nm due to the increase of $DCM\text{-}O^-$ of the pyrolysis product generated by the hydrolysis of DCM-βgal. Therefore, the ratio signal (I_{685nm}/I_{500nm}) increased linearly with the *β*-gal concentration in the range of 0-12 μM (**Figure 9C**). As shown in **Figure 9D**, the FL signal ratio was significantly increased after the addition of *β*-gal, and an approximately 14-fold enhancement in the FL ratio was observed after incubation for 35 min. Furthermore, the probe possessed good specificity for *β*-gal (**Figure 9E**), therefore, the ratiometric FL probe can be used to sense the activity of *β*-gal.

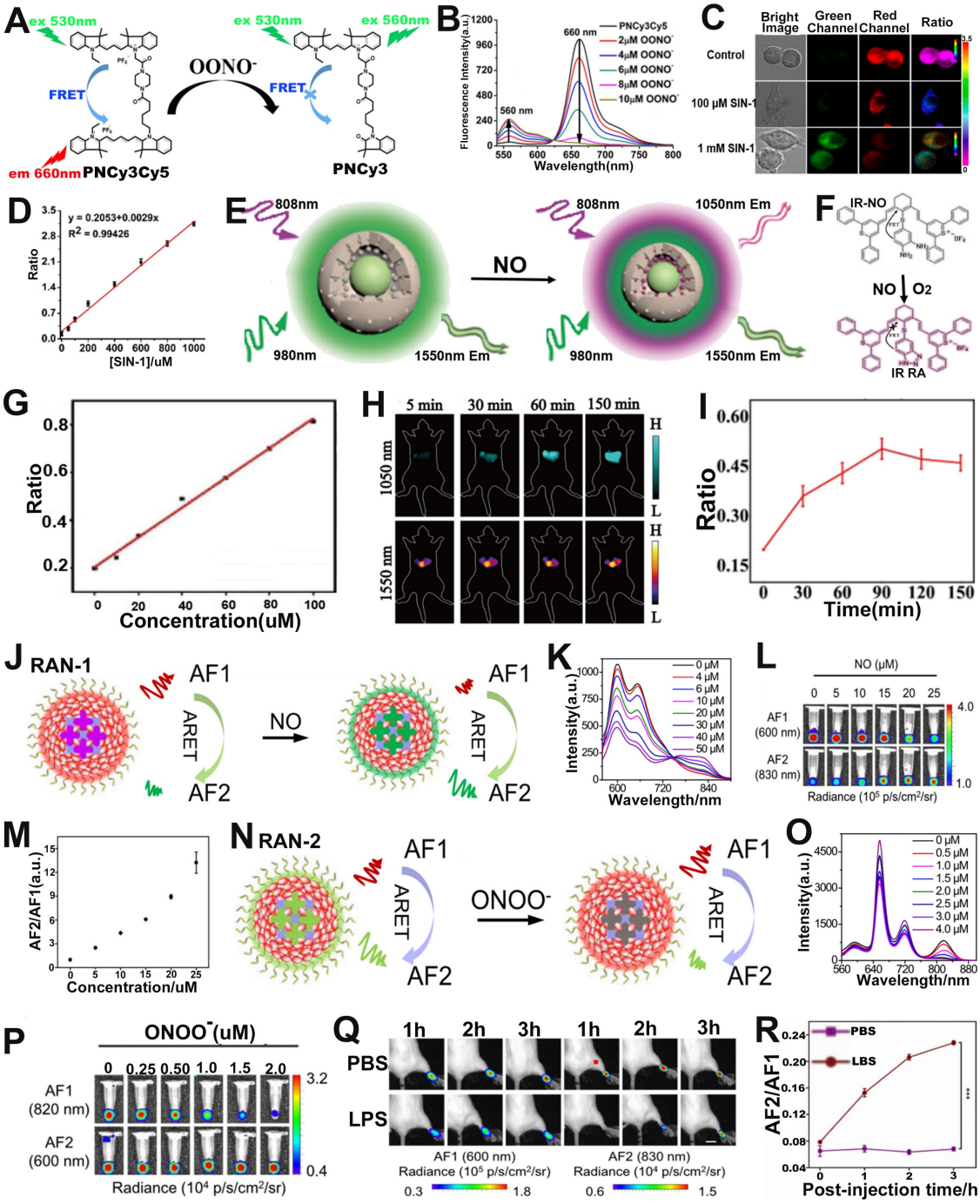

Figure 8. (**A**) Chemical structure and sensing mechanism of PNCy3Cy5 probe. (**B**) FL intensity of PNCy3Cy5 probe after ONOO− activation. (C) Confocal FL imaging of macrophages after different treatments. **(D)** The relationship between SIN-1 concentration and FL signal ratio. (**E**) Schematic illustration of the ratiometric probe for NO sensing. (**F**) Synthetic route and chemical structure of IR-NO. (**G**) Relationship between FL signal ratio and NO concentration. (**H**) Changes in FL images over time after APAP-induced liver injury in mice and (**I**) corresponding FL signal ratio. (**J**) Schematic illustration of ratiometric afterglow RAN-1 probe for NO sensing. (**K**) FL emission spectra of RAN-1 after NO activation. (**L**) Afterglow images of RAN-1 after NO activation. (**M**) Relationship between NO concentration and afterglow signal ratio. (**N**) Schematic illustration of ratiometric afterglow RAN-2 probe for $ONOO^-$ sensing. (**O**) FL emission spectra of RAN-2 after $ONOO^-$ activation. (**P**) Afterglow images of RAN-2 after $ONOO^-$ activation. (**Q**) Changes of afterglow images over time after intravenous administration of RAN-1 in mice pretreated with LPS or PBS, and (**R**) corresponding AF2/AF1. (**A-D**) Adapted with permission from [123], Copyright 2016 American Chemical Society. (**E-I**) Adapted with permission from [124], Copyright 2021 American Chemical Society. (**J-R**) Adapted with permission from [125], Copyright 2022 Springer Nature.

As a typical protease, human neutrophil elastase (HNE), is involved in pathogen destruction and regulation of inflammatory processes in the respiratory tract, and is associated with a variety of lung diseases [131]. Therefore, designing ratiometric optical probes for *in vivo* sensing of HNE will provide a new approach for the clinical diagnosis of lung diseases. The quantum dots (QDs), characterized by high extinction coefficient, wide absorption spectrum and narrow emission spectrum, color tunability, long excited-state lifetime, *etc.*, as FRET donors have been used for the sensing of disease-related biomarkers

[132, 133]. For example, Yang *et al.* developed a retiometric FL probe (QDP) consisting of CdSe/ZnS QDs as the FRET donor, sulforhodamine B (Rh) as the FRET acceptor and HNE-specific oligopeptide substrate (QPMAVVQSVPQK) for sensing of HNE (**Figure 9F**) [134]. The emission spectra of the probe's donor (CdSe/ZnS QDs) overlap a large part of the absorption spectrum of its acceptor (Rh), forming a superior FRET effect. When the QDP probe was incubated with HNE, the amide bond between the two valines of the oligopeptide substrate was hydrolyzed by HNE, resulting in a disruption of the FRET effect, accompanied by a resumption of green FL from the donor and a decrease of red FL from the acceptor (**Figure 9G**). Therefore, the FL signal ratio ($F_{Donor}/F_{Acceptor}$, D/A) increased with increasing HNE concentration. As shown in F**igure 9H**, the QDP probe showed excellent specificity for HNE. When the QDP probe was injected *in situ* into the mouse of lung cancer model, the green FL gradually increased and the red FL gradually decreased at the tumor region as a function of time, leading to a time-dependent FL signal ratio (D/A) increased (**Figure 9I, J**). These results suggested that the FRET-based ratiometric FL probe possessed excellent sensitivity to HNE and, therefore, can be used to sense enzymes that were overexpressed in tumors.

Ye and colleagues developed a γ-glutamyl transpeptidase (GGT) responsive ratiometric FL probe with a FL emission at 517 nm for real-time ratiometric sensing of GGT. The ratiometric FL probe was comprised of GGT responsive cleavable amino acid substrate (γ-Glu), the self-immolation linker 4-amino-benzyl alcohol (PBAB), the quenched-near-infrared fluoresce-Cl, and the always-on BODIPY fluorescein (**Figure 9K**) [135]. Upon incubation with GGT, the γ-Glu in probe was cleaved, subsequently triggered the spontaneous elimination of PBAB, affording a fluorescent product with a new FL emission at 735 nm (**Figure 9L**). As shown in **Figure 9M,** the FL intensity at 735 nm became stronger while at 517 nm remained almost unchanged with the increase of the reaction time between probe and GGT. Therefore, the FL signal ratio (I_{735}/I_{517}) increased as a function of time (**Figure 9N**), and exhibited a GGT concentration dependent I_{735}/I_{517} ratio enhancement (**Figure 9O**). The ratiometric FL probe was incubated with Hela tumor sections and treated with GGT inhibitor (GGsTop) (**Figure 9P**), as shown in **Figure 9Q**, the FL signal ratio of the GGsTop treated group was significantly reduced compared with the GGsTop non-treated group, demonstrating that the probe had excellent GGT responsiveness and was a promising diagnostic tool for GGT sensing.

Sensing of metal ions

Palladium (Pd) is an inert metal that enters the body by residing it in drugs such as gefitinib [136]. When Pd residues enter the human body, excess palladium can lead to disruption of normal cellular functions, which in turn can cause multiple diseases. Recently, ratiometric optical probe has been investigated for sensing of metal ions [137, 138]. For example, Cai *et al*. developed a cyanine fluorophore-based ratiometric PA Pd^{2+} sensor (Cy-DPA) for *in vivo* detection of Pd^{2+} [139]. The ratiometric PA sensor was composed of a heptamethine cyanine as the reporter unit and a dimethylpyridinamine as the recognition unit (**Figure 10A**). As shown in **Figure 10B**, the absorbance of the sensor at 710 nm gradually decreased, while at 770 nm gradually increased with the increase of Pd^{2+} concentration, due to the change of electronic structure after the interaction between Cy-PDA and Pd^{2+}. Therefore, the PA intensity ratio (PA_{770}/PA_{710}) increased with increasing Pd^{2+} concentration (**Figure 10C**). After groin injection of Cy-DPA, the injection region of mice showed a high PA signal at 710 nm and a negligible signal at 770 nm (**Figure 10D**). However, upon Pd^{2+} in solution was injected into the same location, as shown in **Figure 10E**, the signal at 770 nm increased, while at 710 nm decreased. Therefore, the ratiometric PA sensor (Cy-DPA) was effective for *in situ* sensing of Pd^{2+}.

Divalent copper ion (Cu^{2+}) is an essential metal element for the human body, but abnormal copper content can cause numerous serious diseases [140-142]. Therefore, the development of reliable Cu^{2+} sensing methods is of great significance for the diagnosis and treatment of diseases. Chen and colleagues developed a ratiometric PA probe (NRh-IR-NMS) consisting of a selective Cu^{2+} response NRh (as a sensing signal), Cu^{2+} insensitive dye IR (as an internal reference signal) with a PA signal at 834 nm and nanomicelles (NMS) for the sensing of Cu^{2+} *in vivo* (**Figure 10F**) [143]. The NRh-IR-NMS reaction with Cu^{2+} opened the spirolactam ring to generate NRh1 upon treatment with Cu^{2+}, resulting in a significant enhancement of the absorbance at 716 nm (**Figure 10G**). In addition, the NRh-IR-NMS probe showed high selectivity for Cu^{2+} (**Figure 10H**, **I**), and the PA signal ratio (PA_{716}/PA_{834}) increased linearly with the increase of Cu^{2+} concentration (**Figure 10J**). After NRh-IR-NMS probe and Cu^{2+} were co-injected subcutaneously into mice, the PA images at injection region exhibited a Cu^{2+} concentration dependent PA signal ratio (PA_{716}/PA_{834}) enhancement (**Figure 10K**, **L**). These results illustrated that the ratiometric PA probe was an excellent sensing platform for disease diagnosis due to its high selectivity and deep tissue penetration capability.

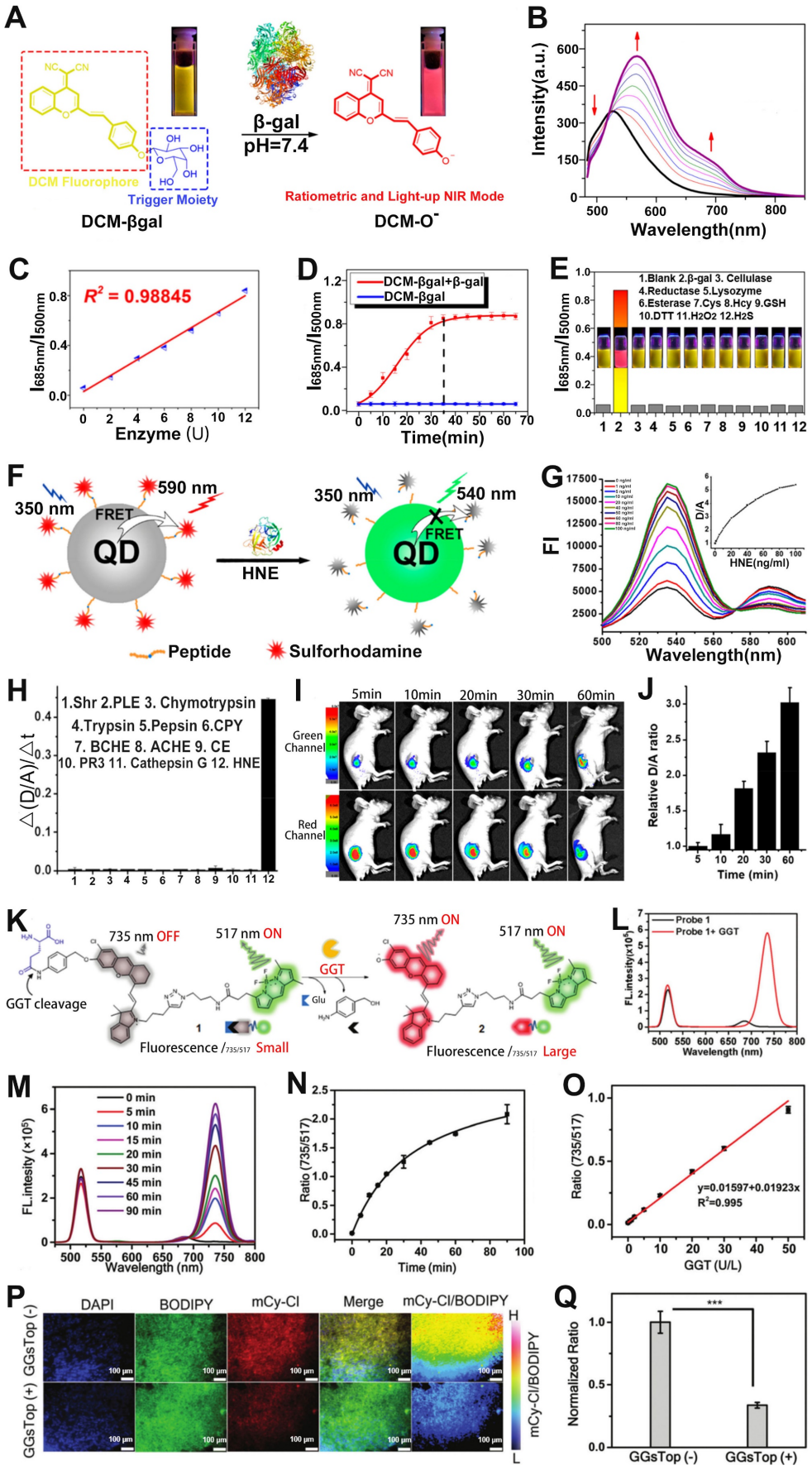

Figure 9. (**A**) Sensing mechanism of DCM-βgal under the action of β-gal enzyme. (**B**) Emission spectrum changes as a function of time. (**C**) Changes in FL signal ratio with increasing enzyme concentration. (**D**) FL signal ratio changes with time before and after addition of β-gal enzyme. (**E**) Changes in the FL ratio after treatment with different

analytes. (**F**) Schematic diagram of sensing principle of QDP probe. (**G**) Changes in the FL spectra after treatment with different concentrations of HNE. (**H**) Changes in signal ratio after different analyte treatments. (**I**) FL images of tumor at different post-injection, and (**J**) corresponding D/A ratio. (**K**) The chemical structure of probe 1 and the principle of enzyme sensing. (**L**) FL spectra of probe after reaction with GGT. (**M**) FL spectra of the probe as a function of time after reaction with GGT. (**N**) Change of FL signal ratio with time. (**O**) The relationship between GGT concentration and FL signal ratio (FL_{735}/FL_{517}). (**P**) FL imaging of GGT activity in tumor tissue sections, and (**Q**) corresponding ratio (FL_{735}/FL_{517}). (**A-E**) Adapted with permission from [130], Copyright 2016 American Chemical Society. (**F-J**) Adapted with permission from [134], Copyright 2020 American Chemical Society. (**K-Q**) Adapted with permission from [135], Copyright 2021 Royal Society of Chemistry.

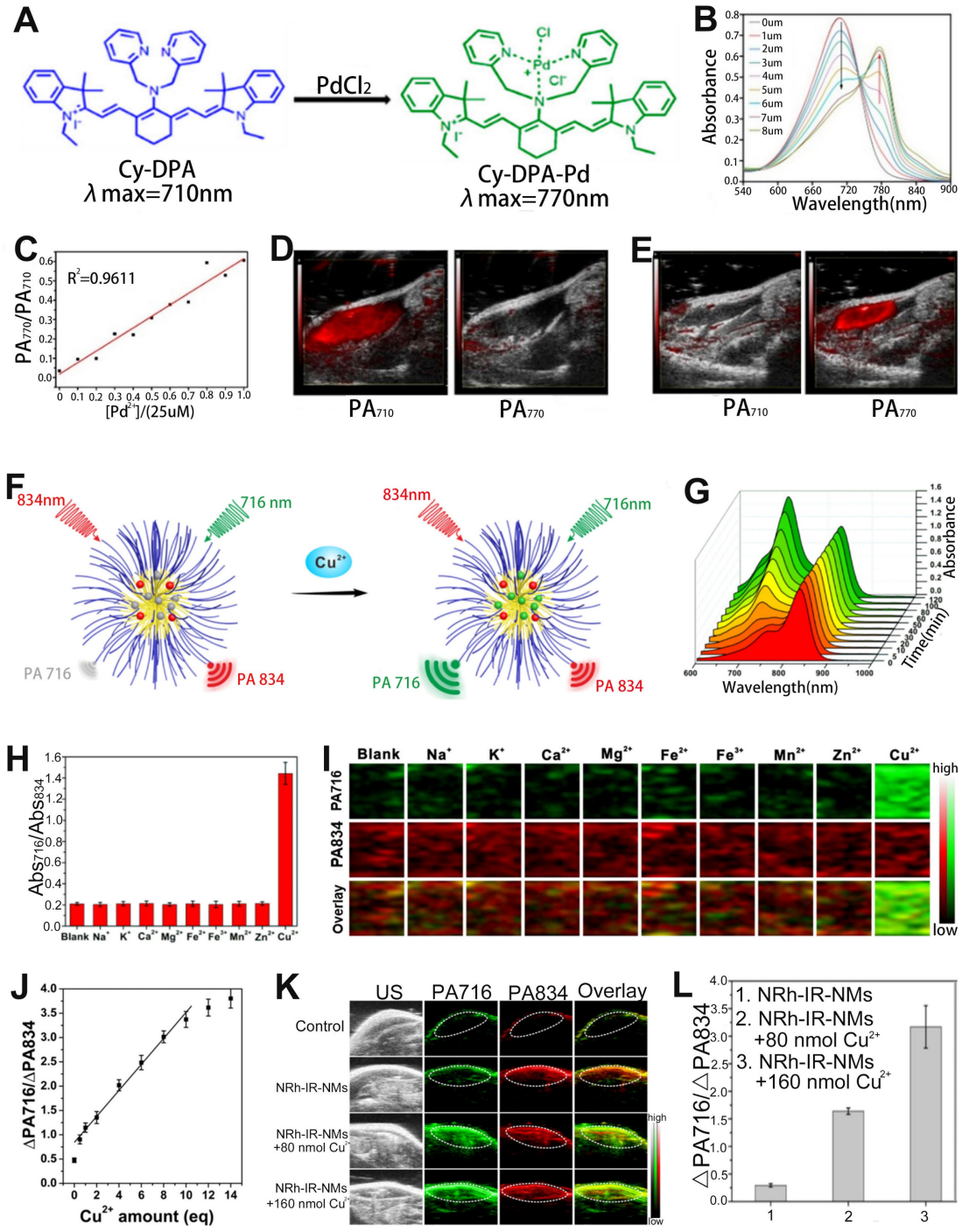

Figure 10. (**A**) Sensing mechanism of Cy-PDA for Pd^{2+}. (**B**) The absorption spectrum of the Cy-PDA after adding different concentrations of Pd^{2+}. (**C**) PA signal ratio (PA_{770}/PA_{710}) as a function of Pd^{2+} concentration. (**D**) PA images at 710 nm and 770 nm after injection of Cy-DPA through the groin in mice. (**E**) PA images at 710 nm and 770 nm after co-injection of Cy-DPA and Pd^{2+} through the groin in mice. (**F**) The sensing mechanism of NRh-IR-NMS for Cu^{2+}. (**G**) Change of absorption spectra of NRh-IR-NM solution with time after adding Cu^{2+} solution. (**H**) Changes in Abs_{716}/Abs_{834} of probes after incubation with different metal ions. (**I**) PA images of NRh-IR-NMS after reaction with metal ions. (**J**) The relationship between Cu^{2+} concentration and PA signal ratio. (**K**) PA images of mice after different treatments and (**L**) corresponding $\Delta PA_{716}/\Delta PA_{834}$. (**A-E**) Adapted with permission from [139], Copyright 2020 American Chemical Society. (**F-L**) Adapted with permission from [143], Copyright 2018 American Chemical Society.

In addition to fluorescent dyes, metal-organic frames (MOFs) prepared by metal ions (or metal clusters) and organic systems with the high sensitivity of luminescence detection and sensing accuracy [144-147] can also realize ratiometric FL sensing of metal ions such as Cu^{2+} and Fe^{3+} by using the ratio of

the two-emission intensity [148, 149].

Sensing of GSH

GSH is involved in the etiology and development of numerous diseases [150, 151]. Therefore, GSH sensing is essential for better disease treatment and understanding of pathological phenomena. Fan and colleagues designed a cyanine derivative-based activatable probe IR806-pyridine dithioethylamine (PDA) consisting of PDA and a disulfide bridged IR806 for real-time sensing of GSH *in vivo* (**Figure 11A, B**) [152]. After incubation with GSH, the disulfide bond of the probe was broken and reduced to sulfydryl group (-SH) due to the extrusion of pyridine, and the product IR806-NH-SH was generated, resulting in wavelength red-shift from 680 nm to 820 nm. Therefore, the PA signal of the probe at 680 nm gradually decreased, while at 820 nm increased with the increase of GSH concentration, resulting in a GSH concentration dependent enhanced PA signal ratio (PA_{820}/PA_{680}) (Figure 11C-E). In addition, the PA signal ratio of GSH treated probe was 12.77-fold and 13.09-fold higher than that of cysteine- and homocysteine-treated probe, respectively. After intravenous injection, ΔPA_{680} increased slightly over time and reached the maximum at 1.5 h post-injection due to the synergistic effect of probe activation leading to a weakened PA signal at 680 nm and probe accumulation in the tumor region, while ΔPA_{820} exhibited a significant increased and reached the plateau at 4 h post-injection (**Figure 11F**). Thus, the PA ratiometric intensity of IR806-PDA in a HeLa tumor model remarkably increased at 4 h post-injection (**Figure 11G**). These results demonstrated that the ratiometric PA probes can be used to specifically sense and identify GSH.

In addition to the ratiometric PA probe, the ratiometric FL probe can also be used to sense GSH. For example, Liu *et al.* developed an activatable ratiometric FL probe (QDs@Cy-GSH) consisting of an organic dyes Cy-GSH, DSPE-PEG and Ag_2Te QDs for sensing of GSH (**Figure 11H**) [153]. The QDs@Cy-GSH probe emitted faint light at 1620 nm under the excitation of 808 nm due to the PET effect from cyanine to the nitroazo group. After the probe was incubated with GSH, GSH replaced the nitro in the probe to form F-SG products, resulting in the elimination of PET effect, hence the FL signal at 1620 nm under 808 nm laser excitation was enhanced, while the FL signal under 980 nm excitation remained unchanged (**Figure 11I, J**). Therefore, the FL signal ratio (I_{808ex}/I_{980ex}) increased as a function of GSH concentration (**Figure 11K, L**). After intravenous administration, the probes were mainly accumulated in the liver because of the overexpression of GSH in the liver. Excess GSH in liver was produced through APAP induced liver injury. After treatment, a stronger I_{808ex}/I_{980ex} in APAP group and weaker I_{808ex}/I_{980ex} in APAP+α-lipoic acid (α-LA) group was observed (**Figure 11M-O**) due to the α-LA inhibited liver toxicity. Therefore, the GSH level could be sensed through the variation of ratiometric FL signal (I_{808ex}/I_{980ex}).

Sensing of Gas molecules

Hydrogen sulfide (H_2S), NO and carbon monoxide (CO) are three endogenous gaseous transmitters that are essential regulators of a variety of physiological and pathological processes [154-156]. Abnormal production of H_2S can cause a variety of diseases. Therefore, designing ratiometric probes to quantitatively sense H_2S *in vivo* is essential for better disease treatment and prognosis. Fan and colleagues developed a chlorinated cyanine dyes based ratiometric PA probe (CyCl-1) for sensing of H_2S *in vivo* through nucleophilic substitution reactions of H_2S with chlorine (**Figure 12A**) [157]. Upon treatment with H_2S, chlorine in the probe was replaced by HS^-, resulting in a change in the color of the probe solution from green to blue due to the ICT effect. In addition, the absorption intensity at 800 nm reduced while that at 720 nm enhanced with the increase of HS^- concentration (**Figure 12B**), resulting in a HS^- concentration dependent PA_{720}/PA_{800} enhancement (**Figure 12C**). After injection of probe into PBS, NaSH and Cys (a precursor of H_2S) treated mice, respectively, the PA signal ratio in NaHS and Cys treated group increased, while that in PBS treated group remained almost unchanged (**Figure 12D, E**), indicating the CyCl-1 probe had excellent responsiveness to H_2S and the correlation between H_2S concentration and PA_{720}/PA_{800} signal ratio enabled quantitative evaluation of endogenous H_2S.

In addition, ratiometric optical probe can be used to sense H_2S in drug-induced liver injury. For example, Song *et al.* developed a H_2S activatable ratiometric PA probe (BDP-H_2S) consisting of aza-BODIPY dye as the signaling moiety and 2,4-dinitrophenyl (DNP) ether as the H_2S responsive moiety for sensing of H_2S in drug-induced liver injury (**Figure 12F**) [158]. The DNP ether, which acted as a strongly electron withdrawing H_2S-responsive moiety, was connected to the Aza-BODIPY scaffold, leading to a blocking of the ICT effect. Upon treatment with H_2S, the ether bond was attacked and broken, and the quaternary ammonium of Aza-BODIPY was converted to tertiary amine. Therefore, the blocked ICT effect was recovered, causing a red-shift of the BDP-H_2S absorption from 770 nm to 840 nm.

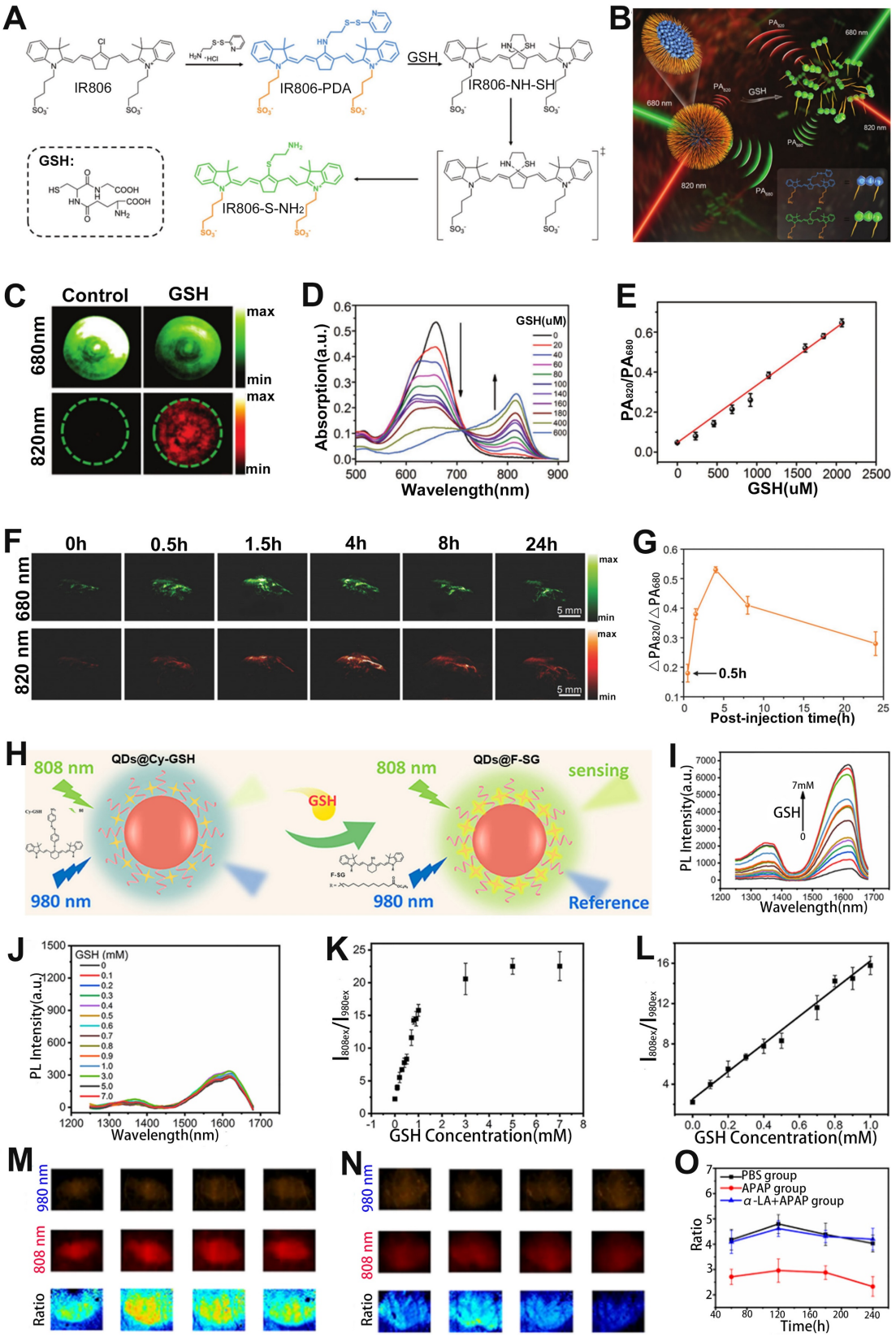

Figure 11. (**A**) Molecular structure of the IR806-PDA probe and the reaction pathway with GSH. (**B**) Proposed mechanism of the ratiometric probe for GSH sensing. (**C**) PA imaging at 680 nm and 820 nm of probes after different treatments. (**D**) GSH responsive UV-vis absorption spectra of IR806-PDA nanoprobe. (**E**) Relationship between GSH concentration and PA signal ratio. (**F**) PA images at different post-injection time. (**G**) Relationship between $\Delta PA_{820}/\Delta PA_{680}$ and post-injection time. (**H**) Schematic illustration of the ratiometric FL probe for sensing of GSH. FL spectra of probe incubated with different concentrations of GSH under excitation at (**I**) 808 nm and (**J**) 980 nm. (**K**) The relationship between FL signal ratio and GSH concentration. (**L**) GSH concentration as a function of FL signal ratio. FL signal intensity in mouse liver treated with (**M**) PBS and (**N**) APAP. (**O**) The change of FL signal ratio (I_{808ex}/I_{980ex}) with time after different treatments. (**A-G**) Adapted with permission from [152], Copyright 2018 WILEY-VCH. (**H-O**) Adapted with permission from [153], Copyright 2021 American Chemical Society.

After the addition of NaHS, the absorption at 770 nm of the probes decreased and at 840 nm increased with increasing NaHS concentration, indicating the BDP-H_2S probe had excellent responsiveness to HS^-. Moreover, the same trend of change occurred for the PA signals (**Figure 12G**). Consequently, the PA signal ratio (PA_{840}/PA_{770}) increased linearly with HS^- concentration (**Figure 12H**). *In vivo* PA imaging in healthy BALB/c mice model and metformin (MET) induced liver injury model (**Figure 12I**) was used to sense H_2S content. As shown in **Figure 12J**, the PA signal ratio (PA_{840}/PA_{770}) of PBS-treated mice was much weaker than that of MET treated mice at 90 min post-injection. The PA_{840}/PA_{770} ratio in the MET-treated group reached a maximum at 50 min post-injection, and the intensity of the ratio was enhanced approximately 2-fold compared to the PBS group, indicating that the BDP-H_2S probe enabled accurate sensing of *in vivo* H_2S level in drug-induced liver injury and had promising application prospects in specific disease-related analytes sensing.

CO, as the second gasotransmitter, is involved in various physiological and pathological processes [159, 160]. For example, it plays a very important role in neurotransmitter regulation, vasodilatation and anti-inflammatory effects [161-163]. However, excessive CO can lead to heart failure (HF), hypertension and many other diseases [164, 165]. It is therefore extremely valuable to develop effective tools to examine *in vivo* CO levels variations with high selectivity and sensitivity. Zhou and co-workers reported a luminescent resonance energy transfer (LRET) effect based ratiometric probe consisting of mesoporous silica ($mSiO_2$)-coated UCNPs ($NaYF_4$@Yb, Er, Tm) with absorption at 543 nm, 658 nm, 801 nm, CO-responsive hemicyanine derivation dye (CyD1) with absorption at 432 nm, and $PdCl_2$ as an additive, for CO sensing *via* upconversion luminescent (UCL) imaging (**Figure 12K**) [166]. CO reduced Pd^{2+} to generate Pd^0 and subsequently mediated the Tsuji-Trost reaction to remove the allylcarbonate group of CyD1, leading to release of CyNH, therefore, the absorption peak was significantly redshifted from 432 nm (CyD1) to 522 nm (CyNH). The increased overlap of the absorption band of CyNH with the emission band of NaYF4@Yb, Er, Tm caused the quenching of the emission at 534 nm (green light) of NaYF4@Yb, Er, Tm, while the emission at 658 nm (red light) remained unchanged as an internal standard (**Figure 12L**). Therefore, the UCL_{543}/UCL_{658} can be used as an output signal for accurate and quantitative sensing of CO. It has been shown that LPS can stimulate the production of endogenous CO. Mice were given saline or LPS intravenously after 12 h, followed by intravenous administration of the probe (**Figure 12M**). A significant decrease in the $UCL_{534\ nm}/UCL_{658\ nm}$ was observed only in the liver of LPS-treated mice, but not in saline-treated controls, due to LPS-induced CO production in the liver region (**Figure 12N, O**). In addition, the $UCL_{534\ nm}/UCL_{658\ nm}$ was reduced approximately 1.64-fold in the LPS-treated mice group compared to the saline-treated mice group. These results demonstrated that the ratiometric probe can be used for sensing of endogenous CO and provide an effective strategy for detecting disease-related gas molecules.

Sensing of hypoxia

Hypoxia is a pathogenic feature of solid tumors due to the absence or abnormal vasculature in the TME, and is essential in tumor progression, angiogenesis, metastasis, invasion, and resistance to immune systems and therapies [167-170]. Therefore, it is of great importance to develop a ratiometric probe for the sensing and quantification of intratumoral hypoxia. Chan et al. designed a hypoxia-responsive ratiometric PA probe (rHyP-1), with a high and low PA signal ratio for hypoxia and normoxia, respectively, for reliable hypoxia sensing (Figure 13A, B) [171]. In vitro ratiometric PA experiments on rHyP-1 indicated that the PA820nm/PA770nm ratio in hypoxia was twice that in normal conditions (Figure 13C-F). Furthermore, the rHyP-1 probe was able to not only sense the intratumor hypoxia, but also predict the region of the tumor where the probe was activated. As shown in Figure 13G, rHyP-1 was used in the sensing of hypoxia in a mouse model of a bearing tumor, where a clear enhancement of PA signal ratios was observed at the injection site, and the PA820nm/PA770nm ratiometric turn-on response relative to the control group increased by a factor of 1.2. In addition, the hypoxic region of tumor can be located via three-dimensional reconstruction ratiometric PA imaging due to the specific activation of the rHyP-1 probe by hypoxia. These results indicated that the ratiometric PA probe can be used to sense and localize the hypoxia in tumor regions.

FRET-based ratiometric probe for immunoassay biosensing

FRET immunoassay is a type of biochemical test that is based on antibody-antigen interactions and allows for the direct and rapid detection of antibody-antigen complex assembly in solution, making it possible to quantify any target of interest in various types of clinical specimens [172, 173]. To perform a FRET immunoassay, two different antibodies are used - one bound to a lanthanide-based donor and the other bound to an appropriate

fluorescent receptor - that separately bind to different epitopes of a target antigen. This brings them into close proximity, enabling FRET. Thus, FRET immunoassay is a powerful tool in molecular diagnostics, with several commercially available brand names, such as HTRF or TRACE, being used clinically to detect different biomarkers [174]. Moreover, time-resolved (TR) or time-gated (TG) FRET immunoassay, which has been used in clinical diagnosis for many years, is particularly useful in its ability to measure fluctuations in FL over time. By combining this with a sensitive detection method, FRET immunoassays can provide highly accurate and reliable diagnostic results for a range of clinical applications [175-177].

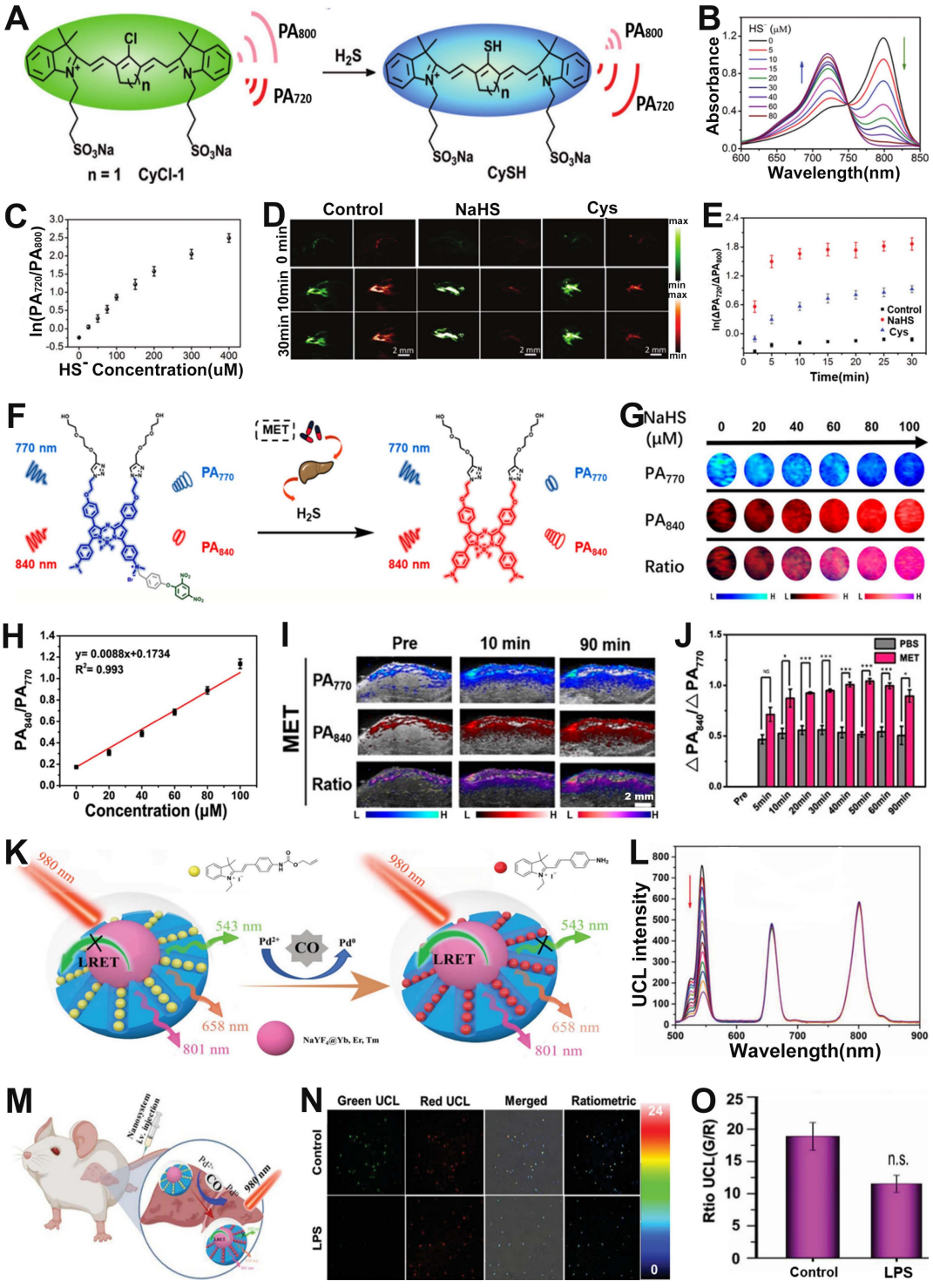

Figure 12. (**A**) Schematic illustration of the structure and sensing principle of CyCl-1 probe. (**B**) Changes in the absorption spectra of probes with increasing HS^- concentration. (**C**) The $\ln(PA_{720}/PA_{800})$ as function of HS^- concentration. (**D**) PA images of mice after different treatments. (**E**) The time-dependent ΔPA signal ratio change. (**F**) Schematic

diagram of the sensing principle of BDP-H_2S probe. (**G**) PA images after treatment with various NaHS concentration, and corresponding (**H**) PA_{840}/PA_{770}. (**I**) PA images of the liver in mice with MET-induced liver injury. (**J**) PA_{840}/PA_{770} in PBS group and MET-induced liver injury group. (**K**) Schematic illustration of the ratiometric UCL probe for CO sensing. (**L**) The absorption spectrum of the ratiometric probe after adding different concentrations of CO. (**M**) Schematic illustration of CO sensing in liver tissues of mouse. (**N**) Ratiometric imaging of endogenous CO in mouse liver tissue after different treatments and (**O**) corresponding $UCL_{534\ nm}/UCL_{658\ nm}$ ratio. (**A-E**) Adapted with permission from [157], Copyright 2019 Royal Society of Chemistry. (**F-J**) Adapted with permission from [158], Copyright 2022 American Chemical Society. (**K-O**) Adapted with permission from [166], Copyright 2022 Wiley-VCH.

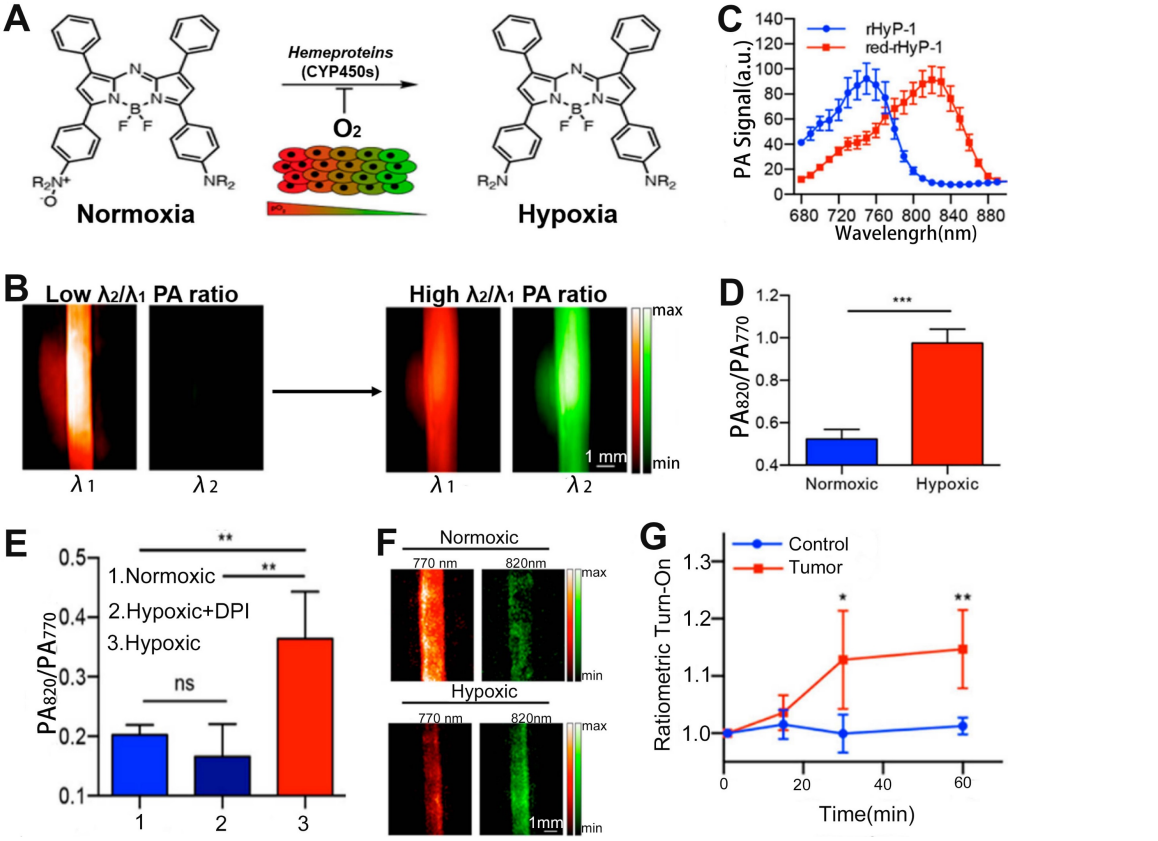

Figure 13. (**A**) Study on the sensing mechanism of probes for hypoxia. (**B**) Changes in PA signal ratio before and after hypoxia. (**C**) PA spectra of rHyP-1 and red rHyP-1. (**D**) Changes in PA signal ratio after 1 h incubation in hypoxic or normoxic conditions. (**E**) Changes of PA signal ratio after different treatment. (**F**) Representative PA images of rHyP-1 probe solutions after incubatiom with rat liver microsomes. (**G**) After rHyP-1 was injected intratumorally or subcutaneously (control) into the tumor-bearing mice, the ratiometric PA turn-on. (**A-G**) Adapted with permission from [171], Copyright 2018 American Chemical Society.

B-type natriuretic peptide (BNP) is a peptide hormone secreted by ventricular cells in response to an increase in ventricular wall tension [178]. Patients with HF have a significant increase in BNP in the blood due to intravascular volume expansion and cardiac pressure overload [179]. Therefore, BNP is considered to be a biomarker of HF. A highly sensitive and specific test for BNP is important for the diagnosis and prognosis of HF patients. Zhang *et al*. developed a FRET-based ratiometric probe for the sensing of BNP based on the competitive binding of graphene oxide (GO) and BNP to its aptamer [180]. The FRET-based ratiometric probe was comprised of GO as the acceptor and a carboxyfluorescein-modified aptamer (FAM-aptamer) with specific recognition of BNP as the donor. GO can bind to FAM-aptamer through hydrophobic interaction and π-π stacking interaction, causing FL signal of FAM-aptamer to be quenched through FRET effect between GO and FAM-aptamer. However, in the presence of the BNP, the BNP preferentially bound to FAM-aptamer and induced a change in the aptamer structure, leading to a separation of GO and FAM-aptamer, after which the FRET effect disappeared and the FL signal of FAM-aptamer was thus restored. Therefore, BNP levels *in vivo* can be sensed by the FL signal ratio ($F_{donor}/F_{acceptor}$). The results indicated that the FRET-based ratiometric probe had good selectivity for BNP and can therefore be used for immunoassay biosensing.

Conclusion and outlook

The ratiometric optical probes and their applications in biosensing have attracted increasing attention over the past decade. Compared to traditional sensing methods for specific disease-related analytes, the ratiometric method enables accurate, real-time sensing with high sensitivity, deep tissue penetration, and self-calibration signal correction. This review systematically summarized and discussed the design strategies and mechanisms of ratiometric optical

probes and their applications in biosensing.

Although current research on ratiometric optical probes is developing rapidly and has made great progress in biosensing, there are endless possibilities for the development of new ratiometric optical probes that meet the sensing needs of different analytes. Accordingly, four research directions deserve our special attention:

(1) Since the same analyte may be present in the pathological microenvironment of different diseases, it is difficult to accurately diagnose a specific disease with a single disease-associated analyte activated ratiometric probe. Therefore, to improve the accuracy and specificity of disease sensing, an effective approach is to design a ratiometric probe that can be used for the sensing of two or multiple biomarkers of a specific disease.

(2) Although ratiometric sensing strategies with a single imaging modality effectively mitigate the problem of the interference of probe's concentration dependent factor, challenges remain due to the limitation of single model imaging. Multimodal ratiometric molecular imaging, such as a single probe with capability of ratiometric PA imaging and ratiometric FL imaging, will be an alternative option for precision medicine in the future. By integrating the advantages of two or multimodal imaging modalities into a single ratiometric probe can minimize the limitations of a single imaging modality and provide more comprehensive information, which is of great value in the diagnosis and treatment of diseases.

(3) Designing a single probe with the ratio between two different imaging modalities could also be a future direction. For example, CL is a self-luminescent imaging method that can avoid the limitations of FL in the presence of strong tissue autofluorescence and light scattering, while FL imaging has high sensitivity and specificity, thus ratiometric CL/FL probe can realize complementary advantages.

(4) Biological barriers in the transport of ratiometric probes hinder biosensing of specific organelles in living cells or target tissues *in vivo*. This process severely limits the bioavailability of the probe at a specific size, which in turn compromises excellent sensing outcomes. The non-specific distribution and inadequate delivery of ratiometric probes are current issues that still need to be addressed. In the next study, ratiometric probes can be rationally combined with innovative targeting design features to overcome biological barriers and realize better sensing performance.

In conclusion, with increasing progress and continuous innovation in materials science and sensing technologies, it is reasonable to believe that ratiometric optical probes are expected to have a broad future in biomedical field.

Abbreviations

ACIE: absorption competition induced emission; AI: afterglow initiator; α-LA: α-lipoic acid; ARET: afterglow resonance energy transfer; BG: bioactive Glass; BL: bioluminescence; BNP: B-type natriuretic peptide; CFP: cyan fluorescent protein; CL: chemiluminescence; CO: carbon monoxide; CRET: chemiluminescence resonance energy transfer; Cu^{2+}: divalent copper ion; CyD1: hemicyanine derivation dye; D-π-A: donor-π-acceptor; DCM: dicyanomethyl-4H-pyran; DCNP: down-conversion nanoparticles; DNP: 2,4-dinitrophenyl; DSPE-PEG: polyethylene glycol phospholipids; ErNPs: Er nanoparticles; EYFP: enhanced yellow fluorescent protein; FAM-aptamer: carboxyfluorescein-modified aptamer; FL: fluorescence; FRET: fluorescence resonance energy transfer; GGsTop: GGT inhibitor; GGT: γ-glutamyl transpeptidase; GM-Ag_2S NDs: co-modified Ag_2S nanodots; GO: graphene oxide; GSH: glutathione; HF: heart failure; H_2S: hydrogen sulfide; HNE: human neutrophil elastase; H_2O_2: hydrogen peroxide; HOCl/HClO: hypochlorous acid; ICT: intramolecular charge transfer; IR-NO: NO-responsive small-molecule organic dye; LPS: lipopolysaccharide; LRET: luminescent resonance energy transfer; MEHPPV: afterglow substrate; MET: metformin; minocycline: $OONO^-$ scavenger; MPA: mercaptopropionic acid; MOFs: metal-organic frames; MPS/mSiO_2: mesoporous silica; mTurquoise2: CFP variant; NIR: near-infrared; NMS: nanomicelles; NO: nitric oxide; $NO_2^{\bullet}$: nitrogen dioxide radicals; NO_3^-: nitrate; NRM: NO-responsive molecule; O_2^-: superoxide; $^1O_2$: singlet state oxygen; ^-OCl: hypochlorite; $^{\cdot}OH$: hydrogen radicals; $ONOO^-$: peroxynitrite; PA: photoacoustic; PBAB: 4-aminobenzyl alcohol; Pd: Palladium; PDA: pyridine dithioethylamine; PEG-b-PPG-b-PEG: amphiphilic triblock copolymer; PET: photoinduced electron transfer; pH-BDP: pH indicator and enhancer; QDs: quantum dots; RAN: ratiometric afterglow probes; Rh: sulforhodamine B; RNS: reactive nitrogen species; ROS: reactive oxygen species; SeTT: NIR-II FL dye; SIN-1: $OONO^-$ donor; SO: semiconducting oligomer; SOA: semiconducting oligomer amphiphile; -SH: sulfydryl group; TG: time-gated; TME: tumor microenvironment; TR: time-resolved; UCL: upconversion luminescent; UCNPs: upconversion nanoparticles; γ-Glu: GGT responsive cleavable amino acid substrate.

Acknowledgements

This work was supported by the Scientific Research of Distinguished Professor from Qingdao

University, China (Grant Number: DC2200000953).

Competing Interests

The authors have declared that no competing interest exists.

References

1. George Kerry R, Ukhurebor KE, Kumari S, Maurya GK, Patra S, Panigrahi B, et al. A comprehensive review on the applications of nano-biosensor-based approaches for non-communicable and communicable disease detection. Biomater Sci. 2021; 9: 3576-602.
2. Bohunicky B, Mousa SA. Biosensors: the new wave in cancer diagnosis. Nanotechnol Sci Appl. 2010; 4: 1-10.
3. Yoo EH, Lee SY. Glucose biosensors: an overview of use in clinical practice. Sensors. 2010; 10: 4558-76.
4. Kim Y, Gonzales J, Zheng Y. Sensitivity-enhancing strategies in optical biosensing. Small. 2021; 17: e2004988.
5. Fahmy HM, Abu Serea ES, Salah-Eldin RE, Al-Hafiry SA, Ali MK, Shalan AE, et al. Recent progress in graphene- and related carbon-nanomaterial-based electrochemical biosensors for early disease detection. ACS Biomater Sci Eng. 2022; 8: 964-1000.
6. Zhong W. Nanomaterials in fluorescence-based biosensing. Anal Bioanal Chem. 2009; 394: 47-59.
7. Zhang C, Yuan Y, Zhang S, Wang Y, Liu Z. Biosensing platform based on fluorescence resonance energy transfer from upconverting nanocrystals to graphene oxide. Angew Chem Int Ed Engl. 2011; 50: 6851-4.
8. Browne KA, Deheyn DD, El-Hiti GA, Smith K, Weeks I. Simultaneous quantification of multiple nucleic acid targets using chemiluminescent probes. J Am Chem Soc. 2011; 133: 14637-48.
9. Fu Q, Yu L, Wang Y, Li P, Song J. Biomarker-responsive nanosystems for chronic disease theranostics. Adv Funct Mater. 2023; 33: 2206300.
10. Yu P, Yan K, Wang S, Yao C, Lei Z, Tang Y, et al. NIR-II dyad-doped ratiometric nanosensor with enhanced spectral fidelity in biological media for in vivo biosensing. Nano Lett. 2022; 22: 9732-40.
11. Bhandari V, Hoey C, Liu LY, Lalonde E, Ray J, Livingstone J, et al. Molecular landmarks of tumor hypoxia across cancer types. Nat Genet. 2019; 51: 308-18.
12. Takahashi S, Piao W, Matsumura Y, Komatsu T, Ueno T, Terai T, et al. Reversible off-on fluorescence probe for hypoxia and imaging of hypoxia-normoxia cycles in live cells. J Am Chem Soc. 2012; 134: 19588-91.
13. Hirasawa T, Iwatate RJ, Kamiya M, Okawa S, Urano Y, Ishihara M. Multispectral photoacoustic imaging of tumours in mice injected with an enzyme-activatable photoacoustic probe. J Opt. 2017; 19: 014002.
14. Jo Y, Kwon J, Kim M, Choi W, Choi M. Microsphere-based interferometric optical probe. Nat Commun. 2018; 9: 4577.
15. Zhu J, Zhu R, Miao Q. Polymeric agents for activatable fluorescence, self-luminescence and photoacoustic imaging. Biosens Bioelectron. 2022; 210: 114330.
16. Jin Y, Xu K, Huang Y, Zhong H, Zhao R. Activity-based probe for ratiometric fluorescence imaging of Caspase-3 in living cells. Anal Chem. 2021; 93: 2045-52.
17. Song X, Li S, Guo H, You W, Shang X, Li R, et al. Graphene-oxide-modified lanthanide nanoprobes for tumor-targeted visible/NIR-II luminescence imaging. Angew Chem Int Ed Engl. 2019; 58: 18981-6.
18. Huang H, Qiu R, Yang H, Ren F, Wu F, Zhang Y, et al. Advanced NIR ratiometric probes for intravital biomedical imaging. Biomed Mater. 2021; 17: 1.
19. Wang X, Zhao X, Zheng K, Guo X, Yan Y, Xu Y. Ratiometric nanoparticle array-based near-infrared fluorescent probes for quantitative protein sensing. Langmuir. 2019; 35: 5599-607.
20. Huang X, Song J, Yung BC, Huang X, Xiong Y, Chen X. Ratiometric optical nanoprobes enable accurate molecular detection and imaging. Chem Soc Rev. 2018; 47: 2873-920.
21. Jin H, Gui R, Yu J, Lv W, Wang Z. Fabrication strategies, sensing modes and analytical applications of ratiometric electrochemical biosensors. Biosens Bioelectron. 2017; 91: 523-37.
22. Lee MH, Kim JS, Sessler JL. Small molecule-based ratiometric fluorescence probes for cations, anions, and biomolecules. Chem Soc Rev. 2015; 44: 4185-91.
23. Chen BB, Liu ML, Zhan L, Li CM, Huang CZ. Terbium(III) modified fluorescent carbon dots for highly selective and sensitive ratiometry of stringent. Anal Chem. 2018; 90: 4003-9.
24. Fu Q, Zhu R, Song J, Yang H, Chen X. Photoacoustic imaging: contrast agents and their biomedical applications. Adv Mater. 2019; 31: e1805875.
25. Choi W, Park B, Choi S, Oh D, Kim J, Kim C. Recent advances in contrast-enhanced photoacoustic imaging: overcoming the physical and practical challenges. Chem Rev. 2023; 123.
26. Ge X, Fu Q, Bai L, Chen B, Wang R, Gao S, et al. Photoacoustic imaging and photothermal therapy in the second near-infrared window. New J Chem. 2019; 43: 8835-51.
27. Wu D, Sedgwick AC, Gunnlaugsson T, Akkaya EU, Yoon J, James TD. Fluorescent chemosensors: the past, present and future. Chem Soc Rev. 2017; 46: 7105-23.
28. Zhao M, Li B, Zhang H, Zhang F. Activatable fluorescence sensors for in vivo bio-detection in the second near-infrared window. Chem Sci. 2020; 12: 3448-59.
29. He S, Li J, Lyu Y, Huang J, Pu K. Near-Infrared fluorescent macromolecular reporters for real-time imaging and urinalysis of cancer immunotherapy. J Am Chem Soc. 2020; 142: 7075-82.
30. Van de Bittner GC, Bertozzi CR, Chang CJ. Strategy for dual-analyte luciferin imaging: in vivo bioluminescence detection of hydrogen peroxide and caspase activity in a murine model of acute inflammation. J Am Chem Soc. 2013; 135: 1783-95.
31. Badr CE, Tannous BA. Bioluminescence imaging: progress and applications. Trends Biotechnol. 2011; 29: 624-33.
32. den Hamer A, Dierickx P, Arts R, de Vries J, Brunsveld L, Merkx M. Bright bioluminescent BRET sensor proteins for measuring intracellular caspase activity. ACS Sens. 2017; 2: 729-34.
33. Su L, Chen Y, Huo H, Liao N, Wu Y, Ge X, et al. NIR-II ratiometric chemiluminescent/fluorescent reporters for real-time monitoring and evaluating cancer photodynamic therapy efficacy. Small. 2022; 18: e2202551.
34. Lu C, Zhang C, Wang P, Zhao Y, Yang Y, Wang Y, et al. Light-free generation of singlet oxygen through manganese-thiophene nanosystems for pH-responsive chemiluminescence imaging and tumor therapy. Chem. 2020; 6: 2314-34.
35. Green O, Gnaim S, Blau R, Eldar-Boock A, Satchi-Fainaro R, Shabat D. Near-Infrared dioxetane luminophores with direct chemiluminescence emission mode. J Am Chem Soc. 2017; 139: 13243-8.
36. Suzuki K, Nagai T. Recent progress in expanding the chemiluminescent toolbox for bioimaging. Curr Opin Biotechnol. 2017; 48: 135-41.
37. Chen W, Zhang Y, Li Q, Jiang Y, Zhou H, Liu Y, et al. Near-Infrared afterglow luminescence of chlorin nanoparticles for ultrasensitive in vivo imaging. J Am Chem Soc. 2022; 144: 6719-26.
38. Li J, Pu K. Development of organic semiconducting materials for deep-tissue optical imaging, phototherapy and photoactivation. Chem Soc Rev. 2019; 48: 38-71.
39. Xu S, Chen R, Zheng C, Huang W. Excited state modulation for organic afterglow: materials and applications. Adv Mater. 2016; 28: 9920-40.
40. Krämer J, Kang R, Grimm LM, De Cola L, Picchetti P, Biedermann F. Molecular probes, chemosensors, and nanosensors for optical detection of biorelevant molecules and ions in aqueous media and biofluids. Chem Rev. 2022; 122: 3459-636.
41. Deng H, Li X, Ju J, Mo X, Ge G, Zhu X. Multifunctional nanoprobes for macrophage imaging. Biomaterials. 2022; 290: 121824.
42. Li Z, Wang C, Zhang M, Li S, Mao Z, Liu Z. Activatable luminescent probes for imaging brain diseases. Nano Today. 2021; 39: 101239.
43. Li W, Wang L, Yin S, Lai H, Yuan L, Zhang X. Engineering a highly selective probe for ratiometric imaging of H_2S_n and revealing its signaling pathway in fatty liver disease. Chem Sci. 2020; 11: 7991-9.
44. Fan X-P, Yang W, Ren T-B, Xu S, Gong X-Y, Zhang X-B, et al. Engineering a ratiometric photoacoustic probe with a hepatocyte-specific targeting ability for liver injury imaging. Anal Chem. 2022; 94: 1474-81.
45. Grootendorst DJ, Jose J, Wouters MW, van Boven H, Van der Hage J, Van Leeuwen TG, et al. First experiences of photoacoustic imaging for detection of melanoma metastases in resected human lymph nodes. Lasers Surg Med. 2012; 44: 541-9.
46. Zheng Y, Liu M, Jiang L. Progress of photoacoustic imaging combined with targeted photoacoustic contrast agents in tumor molecular imaging. Front Chem. 2022; 10: 1077937.
47. Fathi P, Knox HJ, Sar D, Tripathi I, Ostadhossein F, Misra SK, et al. Biodegradable biliverdin nanoparticles for efficient photoacoustic imaging. ACS Nano. 2019; 13: 7690-704.
48. Zhou EY, Knox HJ, Liu C, Zhao W, Chan J. A conformationally restricted Aza-BODIPY platform for stimulus-responsive probes with enhanced photoacoustic properties. J Am Chem Soc. 2019; 141: 17601-9.
49. Lyu Y, Fang Y, Miao Q, Zhen X, Ding D, Pu K. Intraparticle molecular orbital engineering of semiconducting polymer nanoparticles as amplified theranostics for in vivo photoacoustic imaging and photothermal therapy. ACS Nano. 2016; 10: 4472-81.
50. Deán-Ben XL, Gottschalk S, Mc Larney B, Shoham S, Razansky D. Advanced optoacoustic methods for multiscale imaging of in vivo dynamics. Chem Soc Rev. 2017; 46: 2158-98.
51. Lv L, Luo W, Diao Q. A novel ratiometric fluorescent probe for selective detection and imaging of H_2S. Spectrochim Acta A Mol Biomol Spectrosc. 2021; 246: 118959.
52. Haidekker MA, Theodorakis EA. Ratiometric mechanosensitive fluorescent dyes: design and applications. J Mater Chem C Mater. 2016; 4: 2707-18.
53. Ye J, Li Z, Fu Q, Li Q, Zhang X, Su L, et al. Quantitative photoacoustic diagnosis and precise treatment of inflammation in vivo using activatable theranostic nanoprobe. Adv Funct Mater. 2020; 30: 2001771.
54. Vietri MT, Albanese L, Passariello L, D'Elia G, Caliendo G, Molinari AM, et al. Evaluation of neutralizing antibodies after vaccine BNT162b2: preliminary data. J Clin Virol. 2022; 146: 105057.
55. Wang LV, Hu S. Photoacoustic tomography: in vivo imaging from organelles to organs. Science. 2012; 335: 1458-62.
56. Jiang Y, Pu K. Advanced photoacoustic imaging applications of near-infrared absorbing organic nanoparticles. Small. 2017; 13: 1700710.

57. Shen B, Zhang Z, Shi X, Cao C, Zhang Z, Hu Z, et al. Real-time intraoperative glioma diagnosis using fluorescence imaging and deep convolutional neural networks. Eur J Nucl Med Mol Imaging. 2021; 48: 3482-92.
58. Del Rosal B, Ortgies DH, Fernández N, Sanz-Rodríguez F, Jaque D, Rodríguez EM. Overcoming autofluorescence: long-lifetime infrared nanoparticles for time-gated in vivo imaging. Adv Mater. 2016; 28: 10188-93.
59. Lou X, Zhao Z, Tang BZ. Organic dots based on AIEgens for two-photon fluorescence bioimaging. Small. 2016; 12: 6430-50.
60. Foucault-Collet A, Gogick KA, White KA, Villette S, Pallier A, Collet G, et al. Lanthanide near infrared imaging in living cells with Yb^{3+} nano metal organic frameworks. Proc Natl Acad Sci U S A. 2013; 110: 17199-204.
61. Han X, Xu K, Taratula O, Farsad K. Applications of nanoparticles in biomedical imaging. Nanoscale. 2019; 11: 799-819.
62. Gao Y-T, Chen B-B, Jiang L, Lv J, Chang S, Wang Y, et al. Dual-emitting carbonized polymer dots synthesized at room temperature for ratiometric fluorescence sensing of Vitamin B12. ACS Appl Mater Interfaces. 2021; 13: 50228-35.
63. Zhang Y, Hou D, Wang Z, Cai N, Au C. Nanomaterial-based dual-emission ratiometric fluorescent sensors for biosensing and cell imaging. Polymers. 2021; 13.
64. Lin P, Chen D, Zhang L, Xu J, Huang Y, Zhao S. Near-infrared dual-emission ratiometric fluorescence imaging nanoprobe for real-time tracing the generation of endogenous peroxynitrite in single living cells and in vivo. ACS Omega. 2020; 5: 13278-86.
65. Stewart HL, Birch DJS. Fluorescence guided surgery. Methods Appl Fluoresc. 2021; 9: 042002.
66. Wang S, Ren WX, Hou JT, Won M, An J, Chen X, et al. Fluorescence imaging of pathophysiological microenvironments. Chem Soc Rev. 2021; 50: 8887-902.
67. Paraboschi I, De Coppi P, Stoyanov D, Anderson J, Giuliani S. Fluorescence imaging in pediatric surgery: state-of-the-art and future perspectives. J Pediatr Surg. 2021; 56: 655-62.
68. Li Q, Qiao X, Wang F, Li X, Yang J, Liu Y, et al. Encapsulating a single nanoprobe in a multifunctional nanogel for high-fidelity imaging of caspase activity in vivo. Anal Chem. 2019; 91: 13633-8.
69. He J, Hua S, Zhang D, Wang K, Chen X, Zhou M. SERS/NIR-II optical nanoprobes for multidimensional tumor imaging from living subjects, pathology, and single cells and guided NIR-II photothermal therapy. Adv Funct Mater. 2022; 32: 2208028.
70. Fan J, Hu M, Zhan P, Peng X. Energy transfer cassettes based on organic fluorophores: construction and applications in ratiometric sensing. Chem Soc Rev. 2013; 42: 29-43.
71. Zong H, Wang X, Mu X, Wang J, Sun M. Plasmon-enhanced fluorescence resonance energy transfer. Chem Rec. 2019; 19: 818-42.
72. Wu L, Huang C, Emery BP, Sedgwick AC, Bull SD, He X-P, et al. Förster resonance energy transfer (FRET)-based small-molecule sensors and imaging agents. Chem Soc Rev. 2020; 49: 5110-39.
73. Shang J, Yu S, Li R, He Y, Wang Y, Wang F. Bioorthogonal disassembly of hierarchical DNAzyme nanogel for high-performance intracellular microRNA imaging. Nano Lett. 2023.
74. Li X, Yin C, Liew SS, Lee C-S, Pu K. Organic semiconducting luminophores for near-infrared afterglow, chemiluminescence, and bioluminescence imaging. Adv Funct Mater. 2021; 31: 2106154.
75. Thomou T, Mori MA, Dreyfuss JM, Konishi M, Sakaguchi M, Wolfrum C, et al. Adipose-derived circulating miRNAs regulate gene expression in other tissues. Nature. 2017; 542: 450-5.
76. Deroose CM, De A, Loening AM, Chow PL, Ray P, Chatziioannou AF, et al. Multimodality imaging of tumor xenografts and metastases in mice with combined small-animal PET, small-animal CT, and bioluminescence imaging. J Nucl Med. 2007; 48: 295-303.
77. Sato A, Klaunberg B, Tolwani R. In vivo bioluminescence imaging. Comp Med. 2004; 54: 631-4.
78. Welsh DK, Noguchi T. Cellular bioluminescence imaging. Cold Spring Harb Protoc. 2012; 2012.
79. Yan Y, Shi P, Song W, Bi S. Chemiluminescence and bioluminescence imaging for biosensing and therapy: in vitro and in vivo perspectives. Theranostics. 2019; 9: 4047-65.
80. Yang M, Huang J, Fan J, Du J, Pu K, Peng X. Chemiluminescence for bioimaging and therapeutics: recent advances and challenges. Chem Soc Rev. 2020; 49: 6800-15.
81. Dang Q, Jiang Y, Wang J, Wang J, Zhang Q, Zhang M, et al. Room-temperature phosphorescence resonance energy transfer for construction of near-infrared afterglow imaging agents. Adv Mater. 2020; 32: e2006752.
82. le Masne de Chermont Q, Chanéac C, Seguin J, Pellé F, Maîtrejean S, Jolivet JP, et al. Nanoprobes with near-infrared persistent luminescence for in vivo imaging. Proc Natl Acad Sci U S A. 2007; 104: 9266-71.
83. Xu Y, Yang W, Zhang B. ROS-responsive probes for low-background optical imaging: a review. Biomed Mater. 2021; 16: 022002.
84. Jiang X, Lee M, Xia J, Luo T, Liu J, Rodriguez M, et al. Two-Stage SN38 release from a core-shell nanoparticle enhances tumor deposition and antitumor efficacy for synergistic combination with immune checkpoint blockade. ACS Nano. 2022; 16: 21417-30.
85. Arneth B. Tumor microenvironment. Medicina. 2019; 56: 15.
86. Xiao Y, Yu D. Tumor microenvironment as a therapeutic target in cancer. Pharmacol Ther. 2021; 221: 107753.
87. Li Y, Zhao L, Li XF. Hypoxia and the tumor microenvironment. Technol Cancer Res Treat. 2021; 20: 15330338211036304.
88. Li Q, Zeng J, Miao Q, Gao M. Self-illuminating agents for deep-tissue optical imaging. Front Bioeng Biotechnol. 2019; 7: 326.
89. Zhang KY, Yu Q, Wei H, Liu S, Zhao Q, Huang W. Long-lived emissive probes for time-resolved photoluminescence bioimaging and biosensing. Chem Rev. 2018; 118: 1770-839.
90. Wu L, Huang C, Emery BP, Sedgwick AC, Bull SD, He XP, et al. Förster resonance energy transfer (FRET)-based small-molecule sensors and imaging agents. Chem Soc Rev. 2020; 49: 5110-39.
91. Wu YX, Zhang XB, Li JB, Zhang CC, Liang H, Mao GJ, et al. Bispyrene-fluorescein hybrid based FRET cassette: a convenient platform toward ratiometric time-resolved probe for bioanalytical applications. Anal Chem. 2014; 86: 10389-96.
92. Gatenby RA, Gillies RJ. Why do cancers have high aerobic glycolysis? Nat Rev Cancer. 2004; 4: 891-9.
93. Hashim AI, Zhang X, Wojtkowiak JW, Martinez GV, Gillies RJ. Imaging pH and metastasis. NMR Biomed. 2011; 24: 582-91.
94. Pilon-Thomas S, Kodumudi KN, El-Kenawi AE, Russell S, Weber AM, Luddy K, et al. Neutralization of tumor acidity improves antitumor responses to immunotherapy. Cancer Res. 2016; 76: 1381-90.
95. Pini F, Francés-Soriano L, Andrigo V, Natile MM, Hildebrandt N. Optimizing upconversion nanoparticles for FRET biosensing. ACS Nano. 2023; 17: 4971-84.
96. Bhuckory S, Lahtinen S, Höysniemi N, Guo J, Qiu X, Soukka T, et al. Understanding FRET in upconversion nanoparticle nucleic acid biosensors. Nano Lett. 2023; 23: 2253-61.
97. Ding C, Cheng S, Zhang C, Xiong Y, Ye M, Xian Y. Ratiometric upconversion luminescence nanoprobe with near-infrared Ag_2S nanodots as the energy ccceptor for sensing and imaging of pH in vivo. Anal Chem. 2019; 91: 7181-8.
98. Hochreiter B, Garcia AP, Schmid JA. Fluorescent proteins as genetically encoded FRET biosensors in life sciences. Sensors. 2015; 15: 26281-314.
99. Burgstaller S, Bischof H, Gensch T, Stryeck S, Gottschalk B, Ramadani-Muja J, et al. pH-Lemon, a fluorescent protein-based pH reporter for acidic compartments. ACS Sens. 2019; 4: 883-91.
100. Miao Q, Lyu Y, Ding D, Pu K. Semiconducting oligomer nanoparticles as an activatable photoacoustic probe with amplified brightness for in vivo imaging of pH. Adv Mater. 2016; 28: 3662-8.
101. Ryan LS, Gerberich J, Haris U, Nguyen D, Mason RP, Lippert AR. Ratiometric pH imaging using a 1,2-Dioxetane chemiluminescence resonance energy transfer sensor in live animals. ACS Sens. 2020; 5: 2925-32.
102. Sabharwal SS, Schumacker PT. Mitochondrial ROS in cancer: initiators, amplifiers or an achilles' heel? Nat Rev Cancer. 2014; 14: 709-21.
103. Dunnill C, Patton T, Brennan J, Barrett J, Dryden M, Cooke J, et al. Reactive oxygen species (ROS) and wound healing: the functional role of ROS and emerging ROS-modulating technologies for augmentation of the healing process. Int Wound J. 2017; 14: 89-96.
104. MacKay CE, Knock GA. Control of vascular smooth muscle function by Src-family kinases and reactive oxygen species in health and disease. J Physiol. 2015; 593: 3815-28.
105. Barzilai A, Rotman G, Shiloh Y. ATM deficiency and oxidative stress: a new dimension of defective response to DNA damage. DNA Repair. 2002; 1: 3-25.
106. Chen X, Tian X, Shin I, Yoon J. Fluorescent and luminescent probes for detection of reactive oxygen and nitrogen species. Chem Soc Rev. 2011; 40: 4783-804.
107. Pattison DI, Davies MJ. Reactions of myeloperoxidase-derived oxidants with biological substrates: gaining chemical insight into human inflammatory diseases. Curr Med Chem. 2006; 13: 3271-90.
108. Gorrini C, Harris IS, Mak TW. Modulation of oxidative stress as an anticancer strategy. Nat Rev Drug Discov. 2013; 12: 931-47.
109. Yang J, Zhang X, Yuan P, Yang J, Xu Y, Grutzendler J, et al. Oxalate-curcumin-based probe for micro- and macroimaging of reactive oxygen species in Alzheimer's disease. Proc Natl Acad Sci U S A. 2017; 114: 12384-9.
110. Pei P, Hu H, Chen Y, Wang S, Chen J, Ming J, et al. NIR-II ratiometric lanthanide-dye hybrid nanoprobes doped bioscaffolds for in situ bone repair monitoring. Nano Lett. 2022; 22: 783-91.
111. Zhang Y-R, Zhao Z-M, Miao J-Y, Zhao B-X. A ratiometric fluorescence probe based on a novel FRET platform for imaging endogenous HOCl in the living cells. Sens Actuators, B. 2016; 229: 408-13.
112. Ge X, Lou Y, Su L, Chen B, Guo Z, Gao S, et al. Single wavelength laser excitation ratiometric NIR-II fluorescent probe for molecule imaging in vivo. Anal Chem. 2020; 92: 6111-20.
113. Diehn M, Cho RW, Lobo NA, Kalisky T, Dorie MJ, Kulp AN, et al. Association of reactive oxygen species levels and radioresistance in cancer stem cells. Nature. 2009; 458: 780-3.
114. Uttara B, Singh AV, Zamboni P, Mahajan RT. Oxidative stress and neurodegenerative diseases: a review of upstream and downstream antioxidant therapeutic options. Curr Neuropharmacol. 2009; 7: 65-74.
115. Valko M, Leibfritz D, Moncol J, Cronin MT, Mazur M, Telser J. Free radicals and antioxidants in normal physiological functions and human disease. Int J Biochem Cell Biol. 2007; 39: 44-84.
116. Yin C, Zhen X, Fan Q, Huang W, Pu K. Degradable semiconducting oligomer amphiphile for ratiometric photoacoustic imaging of hypochlorite. ACS Nano. 2017; 11: 4174-82.

117. Hirst D, Robson T. Nitric oxide in cancer therapeutics: interaction with cytotoxic chemotherapy. Curr Pharm Des. 2010; 16: 411-20.
118. Bove PF, van der Vliet A. Nitric oxide and reactive nitrogen species in airway epithelial signaling and inflammation. Free radic biol med. 2006; 41: 515-27.
119. Manda-Handzlik A, Bystrzycka W, Cieloch A, Glodkowska-Mrowka E, Jankowska-Steifer E, Heropolitanska-Pliszka E, et al. Nitric oxide and peroxynitrite trigger and enhance release of neutrophil extracellular traps. Cell Mol Life Sci. 2020; 77: 3059-75.
120. Pacher P, Beckman JS, Liaudet L. Nitric oxide and peroxynitrite in health and disease. Physiol Rev. 2007; 87: 315-424.
121. Ferrer-Sueta G, Radi R. Chemical biology of peroxynitrite: kinetics, diffusion, and radicals. ACS Chem Biol. 2009; 4: 161-77.
122. Nagano T. Bioimaging probes for reactive oxygen species and reactive nitrogen species. J Clin Biochem Nutr. 2009; 45: 111-24.
123. Jia X, Chen Q, Yang Y, Tang Y, Wang R, Xu Y, et al. FRET-based mito-specific fluorescent probe for ratiometric detection and imaging of endogenous peroxynitrite: dyad of Cy3 and Cy5. J Am Chem Soc. 2016; 138: 10778-81.
124. Bai F, Du W, Liu X, Su L, Li Z, Chen T, et al. A NO-responsive ratiometric fluorescent nanoprobe for monitoring drug-induced liver injury in the second near-infrared window. Anal Chem. 2021; 93: 15279-87.
125. Liu Y, Teng L, Lyu Y, Song G, Zhang XB, Tan W. Ratiometric afterglow luminescent nanoplatform enables reliable quantification and molecular imaging. Nat Commun. 2022; 13: 2216.
126. Yang K, Zhu L, Nie L, Sun X, Cheng L, Wu C, et al. Visualization of protease activity in vivo using an activatable photo-acoustic imaging probe based on CuS nanoparticles. Theranostics. 2014; 4: 134-41.
127. Dragulescu-Andrasi A, Kothapalli SR, Tikhomirov GA, Rao J, Gambhir SS. Activatable oligomerizable imaging agents for photoacoustic imaging of furin-like activity in living subjects. J Am Chem Soc. 2013; 135: 11015-22.
128. Spergel DJ, Krüth U, Shimshek DR, Sprengel R, Seeburg PH. Using reporter genes to label selected neuronal populations in transgenic mice for gene promoter, anatomical, and physiological studies. Prog Neurobiol. 2001; 63: 673-86.
129. Wei C, Jiang Z, Li C, Li P, Fu Q. Nanomaterials responsive to endogenous biomarkers for cardiovascular disease theranostics. Adv Funct Mater. 2023; 33: 2214655.
130. Gu K, Xu Y, Li H, Guo Z, Zhu S, Zhu S, et al. Real-time tracking and in vivo visualization of β-Galactosidase activity in colorectal tumor with a ratiometric near-infrared fluorescent probe. J Am Chem Soc. 2016; 138: 5334-40.
131. Lucas SD, Costa E, Guedes RC, Moreira R. Targeting COPD: advances on low-molecular-weight inhibitors of human neutrophil elastase. Med Res Rev. 2013; 33 Suppl 1: E73-101.
132. Cardoso Dos Santos M, Algar WR, Medintz IL, Hildebrandt N. Quantum dots for Förster resonance energy transfer (FRET). Trends Analyt Chem. 2020; 125: 115819.
133. Cardoso Dos Santos M, Colin I, Ribeiro Dos Santos G, Susumu K, Demarque M, Medintz IL, et al. Time-gated FRET nanoprobes for autofluorescence-free long-term in vivo imaging of developing zebrafish. Adv Mater. 2020; 32: e2003912.
134. Liu SY, Yan AM, Guo WY, Fang YY, Dong QJ, Li RR, et al. Human neutrophil elastase activated fluorescent probe for pulmonary diseases based on fluorescence resonance energy transfer using CdSe/ZnS quantum dots. ACS Nano. 2020; 14: 4244-54.
135. Huang Z, An R, Wei S, Wang J, Ye D. Noninvasive ratiometric fluorescence imaging of γ-glutamyltransferase activity using an activatable probe. Analyst. 2021; 146: 1865-71.
136. Chinchilla R, Nájera C. Chemicals from alkynes with palladium catalysts. Chem Rev. 2014; 114: 1783-826.
137. Weiss JT, Dawson JC, Fraser C, Rybski W, Torres-Sánchez C, Bradley M, et al. Development and bioorthogonal activation of palladium-labile prodrugs of gemcitabine. J Med Chem. 2014; 57: 5395-404.
138. Carey JS, Laffan D, Thomson C, Williams MT. Analysis of the reactions used for the preparation of drug candidate molecules. Org Biomol Chem. 2006; 4: 2337-47.
139. Xiang J, Liu C, Zhou L, Yang X, Li Y, Jiang Y, et al. Ratiometric photoacoustic chemical sensor for Pd^{2+} ion. Anal Chem. 2020; 92: 4721-5.
140. Cui Z, Bu W, Fan W, Zhang J, Ni D, Liu Y, et al. Sensitive imaging and effective capture of Cu^{2+}: towards highly efficient theranostics of Alzheimer's disease. Biomaterials. 2016; 104: 158-67.
141. Behari M, Pardasani V. Genetics of Wilsons disease. Parkinsonism Relat Disord. 2010; 16: 639-44.
142. Shi Y, Liu Q, Yuan W, Xue M, Feng W, Li F. Dye-assembled upconversion nanocomposite for luminescence ratiometric in vivo bioimaging of copper ions. ACS Appl Mater Interfaces. 2019; 11: 430-6.
143. Wang S, Yu G, Ma Y, Yang Z, Liu Y, Wang J, et al. Ratiometric photoacoustic nanoprobe for bioimaging of Cu^{2}. ACS Appl Mater Interfaces. 2019; 11: 1917-23.
144. Yin H-Q, Yin X-B. Multi-emission from single metal–organic frameworks under single excitation. Small. 2022; 18: 2106587.
145. Yin H-Q, Yin X-B. Metal–organic frameworks with multiple luminescence emissions: designs and applications. Acc Chem Res. 2020; 53: 485-95.
146. Xia Y-D, Sun Y-Q, Cheng Y, Xia Y, Yin X-B. Rational design of dual-ligand Eu-MOF for ratiometric fluorescence sensing Cu^{2+} ions in human serum to diagnose Wilson's disease. Anal Chim Acta. 2022; 1204: 339731.
147. Yin X-B, Sun Y-Q, Yu H, Cheng Y, Wen C. Design and multiple applications of mixed-ligand Metal–Organic Frameworks with dual emission. Anal Chem. 2022; 94: 4938-47.
148. Chen L, Liu D, Peng J, Du Q, He H. Ratiometric fluorescence sensing of metal-organic frameworks: tactics and perspectives. Coord Chem Rev. 2020; 404: 213113.
149. Wei W, Zhang Y-R, Yin X-B, Xia Y. Multifunctional AIEgen-based luminescent metal–organic frameworks with coordination-induced emission for chemical sensing. New J Chem. 2022; 46: 9641-9.
150. Balendiran GK, Dabur R, Fraser D. The role of glutathione in cancer. Cell Biochem Funct. 2004; 22: 343-52.
151. Yang P, Ebbert JO, Sun Z, Weinshilboum RM. Role of the glutathione metabolic pathway in lung cancer treatment and prognosis: a review. J Clin Oncol. 2006; 24: 1761-9.
152. Yin C, Tang Y, Li X, Yang Z, Li J, Li X, et al. A single composition architecture-based nanoprobe for ratiometric photoacoustic imaging of Glutathione (GSH) in living mice. Small. 2018; 14: e1703400.
153. Song D, Zhu M, Li C, Zhou Y, Xie Y, Li Z, et al. Boosting and cctivating NIR-IIb luminescence of Ag_2Te quantum dots with a molecular trigger. Anal Chem. 2021; 93: 16932-9.
154. Szabó C. Hydrogen sulphide and its therapeutic potential. Nat Rev Drug Discov. 2007; 6: 917-35.
155. Lefer DJ. A new gaseous signaling molecule emerges: cardioprotective role of hydrogen sulfide. Proc Natl Acad Sci U S A. 2007; 104: 17907-8.
156. Kimura H. Signaling of hydrogen sulfide and polysulfides. Antioxid Redox Signal. 2015; 22: 347-9.
157. Li X, Tang Y, Li J, Hu X, Yin C, Yang Z, et al. A small-molecule probe for ratiometric photoacoustic imaging of hydrogen sulfide in living mice. Chem Commun. 2019; 55: 5934-7.
158. Wu R, Chen Z, Huo H, Chen L, Su L, Zhang X, et al. Ratiometric detection of H_2S in liver injury by activated two-wavelength photoacoustic imaging. Anal Chem. 2022; 94: 10797-804.
159. Powell CR, Dillon KM, Matson JB. A review of hydrogen sulfide (H_2S) donors: chemistry and potential therapeutic applications. Biochem Pharmacol. 2018; 149: 110-23.
160. Siracusa R, Schaufler A, Calabrese V, Fuller PM, Otterbein LE. Carbon monoxide: from poison to clinical trials. Trends Pharmacol Sci. 2021; 42: 329-39.
161. Verma A, Hirsch DJ, Glatt CE, Ronnett GV, Snyder SH. Carbon monoxide: a putative neural messenger. Science. 1993; 259: 381-4.
162. Romão CC, Blättler WA, Seixas JD, Bernardes GJ. Developing drug molecules for therapy with carbon monoxide. Chem Soc Rev. 2012; 41: 3571-83.
163. Qian Y, Matson JB. Gasotransmitter delivery via self-assembling peptides: treating diseases with natural signaling gases. Adv Drug Delivery Rev. 2017; 110-111: 137-56.
164. Ryter SW, Alam J, Choi AM. Heme oxygenase-1/carbon monoxide: from basic science to therapeutic applications. Physiol Rev. 2006; 86: 583-650.
165. Schroeder RA, Ewing CA, Sitzmann JV, Kuo PC. Pulmonary expression of iNOS and HO-1 protein is upregulated in a rat model of prehepatic portal hypertension. Dig Dis Sci. 2000; 45: 2405-10.
166. Ye M, Zhang J, Jiang D, Tan Q, Li J, Yao C, et al. A hemicyanine-assembled upconversion nanosystem for NIR-excited visualization of carbon monoxide bio-signaling in vivo. Small. 2022; 18: e2202263.
167. Bouleftour W, Rowinski E, Louati S, Sotton S, Wozny AS, Moreno-Acosta P, et al. A review of the role of hypoxia in radioresistance in cancer therapy. Med Sci Monit. 2021; 27: e934116.
168. Rakotomalala A, Escande A, Furlan A, Meignan S, Lartigau E. Hypoxia in solid tumors: how low oxygenation impacts the "Six Rs" of radiotherapy. Front Endocrinol. 2021; 12: 742215.
169. Zhang S, Chen H, Wang L, Qin X, Jiang B-P, Ji S-C, et al. A general approach to design dual ratiometric fluorescent and photoacoustic probes for quantitatively visualizing tumor hypoxia levels in vivo. Angew Chem Int Ed. 2022; 61: e202107076.
170. Takahashi S, Piao W, Matsumura Y, Komatsu T, Ueno T, Terai T, et al. Reversible off–on fluorescence probe for hypoxia and imaging of hypoxia–normoxia cycles in live cells. J Am Chem Soc. 2012; 134: 19588-91.
171. Knox HJ, Kim TW, Zhu Z, Chan J. Photophysical tuning of n-oxide-based probes enables ratiometric photoacoustic imaging of tumor hypoxia. ACS Chem Biol. 2018; 13: 1838-43.
172. Wang B, Park B. Immunoassay biosensing of foodborne pathogens with surface plasmon resonance imaging: a review. J Agric Food Chem. 2020; 68: 12927-39.
173. Hameed S, Xie L, Ying Y. Conventional and emerging detection techniques for pathogenic bacteria in food science: a review. Trends Food Sci Technol. 2018; 81: 61-73.
174. Qiu X, Hildebrandt N. A clinical role for Förster resonance energy transfer in molecular diagnostics of disease. Expert Rev Mol Diagn. 2019; 19: 767-71.
175. Hildebrandt N, Wegner KD, Algar WR. Luminescent terbium complexes: superior Förster resonance energy transfer donors for flexible and sensitive multiplexed biosensing. Coord Chem Rev. 2014; 273-274: 125-38.
176. Qiu X, Xu J, Cardoso Dos Santos M, Hildebrandt N. Multiplexed biosensing and bioimaging using lanthanide-based time-gated Förster resonance energy transfer. Acc Chem Res. 2022; 55: 551-64.
177. Francés-Soriano L, Leino M, Dos Santos MC, Kovacs D, Borbas KE, Söderberg O, et al. In situ rolling circle amplification Förster resonance energy transfer

(RCA-FRET) for washing-free real-time single-protein imaging. Anal Chem. 2021; 93: 1842-50.
178. Richards AM. N-terminal B-type natriuretic peptide in heart failure. Heart failure clinics. 2018; 14: 27-39.
179. Lei YM, Xiao MM, Li YT, Xu L, Zhang H, Zhang ZY, et al. Detection of heart failure-related biomarker in whole blood with graphene field effect transistor biosensor. Biosens Bioelectron. 2017; 91: 1-7.
180. Tu A, Shang J, Wang Y, Li D, Liu L, Gan Z, et al. Detection of B-type natriuretic peptide by establishing a low-cost and replicable fluorescence resonance energy transfer platform. Mikrochim Acta. 2020; 187: 331.